Redox Biology 69 (2024) 102983

Contents lists available at ScienceDirect

Redox Biology

journal homepage: www.elsevier.com/locate/redox

# Shank3 ameliorates neuronal injury after cerebral ischemia/reperfusion via inhibiting oxidative stress and inflammation

Hongchen Zhang [a,1], Yuan Feng [a,1], Yanfang Si [b,1], Chuanhao Lu [a], Juan Wang [a], Shiquan Wang [a], Liang Li [a], Wenyu Xie [a], Zheming Yue [a], Jia Yong [a], Shuhui Dai [a,c,***], Lei Zhang [a,**], Xia Li [a,*]

[a] Department of Neurosurgery, Xijing Hospital, Fourth Military Medical University, Xi'an, 710032, China
[b] Department of Ophthalmology, The Eighth Medical Center, Affiliated to the Senior Department of Ophthalmology, The Third Medical Center, Chinese People's Liberation Army General Hospital, Beijing, 100091, China
[c] National Translational Science Center for Molecular Medicine and Department of Cell Biology, Fourth Military Medical University, Xi'an, 710032, China

ARTICLE INFO

*Keywords:*
Shank3
STIM1
Ischemia/reperfusion injury
Oxidative stress
Inflammation

ABSTRACT

Shank3, a key molecule related to the development and deterioration of autism, has recently been found to downregulate in the murine brain after ischemia/reperfusion (I/R). Despite this discovery, however, its effects on neuronal injury and the mechanism underlying the effects remain to be clarified. To address this, in this study, based on genetically modified mice models, we revealed that the expression of Shank3 showed a time-dependent change in murine hippocampal neurons after I/R, and that conditional knockout (cko) of Shank3 in neurons resulted in aggravated neuronal injuries. The protective effects of Shank3 against oxidative stress and inflammation after I/R were achieved through direct binding STIM1 and subsequent proteasome-mediated degradation of STIM1. The STIM1 downregulation induced the phosphorylation of downstream Nrf2 Ser40, which subsequently translocated to the nucleus, and further increased the expression of antioxidant genes such as NQO1 and HO-1 in HT22 cells. *In vivo*, the study has further confirmed that double knockout of Shank3 and Stim1 alleviated oxidative stress and inflammation after I/R in Shank3$^{cko}$ mice. In conclusion, the present study has demonstrated that Shank3 interacts with STIM1 and inhibits post-I/R neuronal oxidative stress and inflammatory response via the Nrf2 pathway. This interaction can potentially contribute to the development of a promising method for I/R treatment.

## 1. Introduction

Brain ischemic stroke (IS) is one of the leading causes of death and disability worldwide [1,2]. With the increasing application of endovascular recanalization technology and thrombolytic drugs, neuronal injury caused by ischemia/reperfusion (I/R) has become a critical issue that needs to be addressed in neuroscience [3]. Hippocampus is highly vulnerable to ischemia [4–6], which contains rescuable damaged neurons. Much evidence suggests that oxidative stress, inflammation, and glutamate excitotoxicity underlying I/R-induced secondary neuronal injury [7,8]. This is largely due to the excessive accumulation of reactive oxygen species (ROS), which not only lead to the destruction of cellular macromolecules, increased DNA damage, protein oxidation, and lipid peroxidation, but also aggravate the inflammatory response [9,10]. Such a cascade of events further induces neuronal apoptosis or necrosis after I/R [11–13].

Shank3, as a member of family of the extremely conserved ProSAP/Shank synaptic scaffolding proteins [14], has been found to be associated with various central nervous system diseases, including autism spectrum disorders, Alzheimer's disease, and depression by regulating synaptic plasticity of neuronal circuits [15–18]. Predominantly localized in the postsynaptic density (PSD) of neurons, Shank3 forms complexes with metabotropic glutamate receptors (mGluRs) and Homer1a proteins [19–21]. Shank3 also activates downstream signaling molecules, such as calcium/calmodulin-dependent protein kinase type II (CaMKII) to regulate calcium concentrations, PSD assembly, and dendritic spine

* Corresponding author. Department of Neurosurgery, Xijing Hospital, Fourth Military Medical University, 127 Changlexi Rd, Xi'an, 710032, China.
** Corresponding author. Department of Neurosurgery, Xijing Hospital, Fourth Military Medical University, 127 Changlexi Rd, Xi'an, 710032, China.
*** Corresponding author. Department of Neurosurgery, Xijing Hospital, Fourth Military Medical University, 127 Changlexi Rd, Xi'an, 710032, China.
*E-mail addresses:* dsh20012004@163.com (S. Dai), zhangleiafmmu@163.com (L. Zhang), lixia_fmmu@163.com (X. Li).
[1] Hongchen Zhang, Yuan Feng, and Yanfang Si have contributed equally to this work.

https://doi.org/10.1016/j.redox.2023.102983
Received 16 October 2023; Received in revised form 22 November 2023; Accepted 30 November 2023
Available online 5 December 2023
2213-2317/© 2023 The Authors. Published by Elsevier B.V. This is an open access article under the CC BY-NC-ND license (http://creativecommons.org/licenses/by-nc-nd/4.0/).

morphology [22,23]. Although Datta AQ first found in 2011 that Shank3 expression in rat brains downregulated after I/R [24], the influence of Shank3 on neuronal I/R injury is yet to be fully elucidated.

Stromal interactive molecules 1 (STIM1) is a calcium ion sensor localized on the endoplasmic reticulum membrane [25]. Our previous studies [26–28] have proven that, after oxidative stress injury in neurons, STIM1 expression increases and then leads to intracellular calcium overload and mitochondrial dysfunction, which in turn induced ROS accumulation and neuronal apoptosis. Moreover, we have also observed that overexpression of Homer1a attenuated the toxic effects of glutamate on neurons by inhibiting STIM1-mediated calcium overload, indicating that STIM1 and Homer1a work in tandem during the neuronal oxidative stress and excitotoxic injury. There is a lot of evidence demonstrating that nuclear factor erythroid 2-related factor 2 (Nrf2) plays a central role in regulating the antioxidant response within the body [29] as it can upregulate the expression of antioxidant proteins such as NAD(P)H dehydrogenase quinone 1 (NQO1) and heme oxygenase-1 (HO-1), further lower ROS levels, and inhibit post-IR neuronal injuries [30,31]. However, whether the protective effects of Nrf2 is related to STIM1 has yet to be demonstrated.

The present study was intended to explore the role and underlying mechanism of Shank3 in hippocampal neuronal injury following I/R. Our study showed that Shank3 expression in hippocampal neurons after I/R changed in a time-dependent manner, and conditional knockout of Shank3 in neurons significantly aggravated neurological function deficits. We further confirmed that Shank3 regulated neuronal oxidative stress and inflammatory activity after I/R via the STIM1/Nrf2 pathway. These findings may potentially contribute to the development of a promising new therapeutic strategy for I/R.

## 2. Materials and methods

### 2.1. Ethics

All the animal experiments were approved by the Institutional Animal Care and Use Committee of the Fourth Military Medical University (Xi'an, China). All animal handling procedures and experimental protocols were performed according to the National Institutes of Health (NIH) guidelines for the use of experimental animals.

### 2.2. Animals

72 adult male C57BL/6 mice (20–25 g, 8-week old) were purchased from the Experimental Animal Center of the Fourth Military Medical University (Xi'an, China). 240 Shank3$^{flox/flox}$/Emx1-Cre$^{+/-}$ (Shank3$^{cko}$) (20–25 g, 8-week old) on C57BL/6 genetic background were generated at Cyagen Biosciences Inc. Mice were housed in standard cages and under controlled environmental conditions with a consistent temperature of 22–25 °C, relative humidity of 65 % and 12 h light/dark cycle, and were allowed free access to food and water. Transgenic mice were identified by polymerase chain reaction analysis (PCRA) of genomic DNA in the tail using the following primers:

Shank3 floxed (forward: 5′-TTTTCTGTCTGTGGTATAAGCTGC-3′, reverse: 5′-CTATGACATGACTTTGCCTTCCAG-3′);

Cre (forward1: 5′-TTCCTCCTCTCCTGACTACTCCCAG-3′, forward2: 5′- GTGAAGGTGTGGTTCCAGAATCGG-3' , reverse: 5′-CTCTTGTCCCTCTGACAGTGATGGC-3′).

### 2.3. Transient middle cerebral artery occlusion (tMCAO) model

The tMCAO model was constructed according to previously published methods [32]. Mice were anesthetized with 5 % isoflurane and the anesthesia was maintained at a level of 2 % isoflurane during the surgery. Buprenorphine (0.1 mg/kg, subcutaneously injection) was administered 1 h before surgery. Body temperature was maintained at 37 °C with a heating pad. The right external carotid artery (ECA) was isolated and a standardized nylon filament (RWD Life Science, Cat# MSMC21B120PK50, China) inserted into the origin of the right middle cerebral artery (MCA) via the right internal carotid artery (ICA). The filament was removed to allow reperfusion 60 min after surgery. Cortical cerebral blood flow (CBF) was recorded using a laser Doppler flowmeter (RFLSI III, RWD Life Science, China), with the reduction of blood flow to 20 % of the baseline being considered successful occlusion. Mice in the Sham group underwent the same procedure except for filament insertion.

### 2.4. Experimental grouping

54 C57BL/6 mice were randomized into Sham group [12] and tMCAO group [60]. The brain tissues of 6 mice per group were collected at 60 min after tMCAO, and 3, 6, 12, and 24 h after reperfusion for further experiments. Additionally, 6 mice in the Sham group, Ischemia (1 h) group, and I/R (24 h) group were sacrificed to obtain frozen sections for pathological experiments. The detection index of the three microscopic regions randomly selected from one section of each mouse was quantified and averaged.

In subsequent experiments, 80 Shank3$^{flox/flox}$ (Shank3$^{f/f}$) were randomly assigned to the following experiment groups: [1] Sham + Shank3$^{f/f}$ and [2] I/R + Shank3$^{f/f}$. 156 Shank3$^{cko}$ mice were randomly assigned to the following experimental groups: [1] Sham + Shank3$^{cko}$, [2] I/R + Shank3$^{cko}$, [3] I/R + Shank3$^{cko}$ + vehicle, [4] I/R + Shank3$^{cko}$ + sgSTIM1.

### 2.5. Neurological deficit evaluation

The Clark score consisting of focal and general parts was performed to evaluate the neurological deficits [33]. The focal part contained 7 items with a total score of 28 points. The general part had 6 items with a total score of 28 points as well. Higher scores are usually indicative of more serious neurological deficits.

### 2.6. Infarction volume

We performed 2,3,5-Triphenyltetrazolium hydrochloride (TTC) staining to evaluate the infarction volume. Mouse brains were harvested immediately after sacrifice and sliced 2 mm sections (model No. 68707, RWD Life Science, China). The brain sections were incubated with 2 % TTC (Sigma-Aldrich, Cat# T8877, USA) at 37 °C for 30 min in the dark. Stained brain sections were fixed in 2 % paraformaldehyde and photographed. The percentage of infarction volume (white) was analyzed using Image J software (NIH).

### 2.7. Brain water content measurement

The fresh brain tissues were weighed to obtain the wet weight (WW) which was followed by dehydration at 105 °C consistently for 24 h to determine the dry weight (DW). Brain water content was calculated using the following formula: (WW - DW)/WW × 100 %.

### 2.8. Quantitative real-time PCR (qPCR) analysis

Total RNA was extracted using TRIzol™ reagent (Thermo Fisher Scientific, Cat# 15596018, USA). Standard cDNA synthesis reactions and reverse transcription were carried out using PrimeScript™ RT Master Mix (TaKaRa, Cat# RR036, Japan) according to the manufacturer's instructions. For RT-qPCR analysis, reverse transcribed products were amplified using TB Green™ Premix Ex Taq™ II Kit (TaKaRa, Cat# RR820, Japan). Relative mRNA levels were determined by the CFX96 Touch Real-Time PCR Detection System (Biorad, USA). The relative expression level (defined as fold change) was determined using the $2^{-\Delta\Delta Ct}$ method. The following primers were used:

Shank3 (forward: 5′-ACGAAGTGCCTGCGTCTGGAC-3′, reverse: 5′-

CTCTTGCCAACCATTCTCATCAGTG-3′);

β-actin (forward: 5′-CATCCGTAAAGACCTCTATGCCAAC-3′, reverse: 5′-ATGGAGCCACCGATCCACA-3′).

### 2.9. RNA sequencing (RNA-Seq)

The total RNA of Shank3 cko mice hippocampal brain tissue was extracted using TRIzol reagent (Invitrogen, Cat# 15596026, USA) according to the manufacturer's protocol. RNA quality was analyzed using Agilent 2100 Bioanalyzer (Agilent Technologies, USA). Then eukaryotic mRNA was enriched with Oligo (dT) beads. The short fragments of the enriched mRNA were fragmented with a fragmentation buffer and reverse transcripted into cDNA using random primers. DNA polymerase I, RNase H, dNTP, and buffer facilitated the synthesis of second-strand cDNA. The resulting cDNA fragments were purified with a QiaQuick PCR extraction kit (Qiagen, Venlo, The Netherlands), end-repaired, poly (A) added, and ligated to Illumina sequencing adapters. Then the ligation products were size selected by agarose gel electrophoresis, PCR amplified, and sequenced on Illumina Novaseq6000 by Gene Denovo Biotechnology Co. (China). After RNA-Seq, Gene Ontology (GO) analysis and gene set enrichment analysis (GSEA) were carried out.

### 2.10. Cell culture and oxygen and glucose deprivation/reperfusion (OGD/R) model

Murine hippocampal neuron HT22 cells were cultured in Dulbecco's Modified Eagle's Medium (DMEM) containing 10 % fetal bovine serum and antibiotics (penicillin, 100 IU/ml, streptomycin, 100 μg/ml) at 37 °C in a standard cell incubator with 5 % $CO_2$ and 95 % $O_2$ before oxygen and glucose deprivation. To construct the OGD/R model, the HT22 cells were cultured in glucose-free DMEM and placed into a specialized, humidified chamber containing 5 % $CO_2$, and 95 % $N_2$ at 37 °C. After 8 h, the cells were removed from the anaerobic chamber to the regular incubator, and the culture medium was replaced with a standard culture medium for 24 h at 37 °C to generate the reperfusion insult.

### 2.11. Gene knockdown and overexpression in vitro

To knockdown Shank3 expression in *vitro*, the lentiviral vector GV493 (hU6-MCS-CBh-gcGFP-IRES-puromycin, GeneChem, China) was used to deliver the short hairpin RNA (shRNA) targeting the mouse *Shank3* sequences (GAGGTAATCAAGACCCACAAA), and non-silencing negative control (NC, TTCTCCGAACGTGTCACGT). HT22 cells were infected with the concentrated lentivirus and allowed to recover in fresh serum-containing DMEM medium for 48 h to permit Shank3 knockdown. For Shank3 overexpression experiments, cDNAs of the mouse *Shank3* gene were cloned into a GV747 lentiviral vector (CMV enhancer-MCS-T2A-puromycin, GeneChem, China). The viruses were packaged into the HEK 293T cell line, and viral culture supernatants were harvested and concentrated after transfection for 48 h. To determine the effects of STIM1, the pre-designed small interfering RNA (siRNA) directed against STIM1 (GCAGGTAGGAGAGTGTACAGGATGCCTT) and negative control (NC, UUCUCCGAACGUGUCACGUTT) were chemically synthesized by Genechem Company (China) and then were used to measure the off-target effect. Transfection was performed using the Lipofectamine RNAiMAX Transfection Reagent (Thermo Fisher Scientific, Cat# 13778100, USA) according to the manufacturer's instructions. Cells were cultured in fresh DMEM medium and harvested 48 h after transfection.

### 2.12. Intra-hippocampus injection of CAS9-KO-adeno-associated virus (AAV)

To knockdown STIM1 expression *in vivo*, the small guide RNA (sgRNA) for mouse *Stim1* (GAAGGGTTACACGGGCTGAG) was packaged into a recombinant adeno-associated virus vector GV487 (CMV-NLS-SaCas9-NLS-3xHA-bGHpA-U6-sgRNA, serotype 9, GeneChem, China). AAV9-Stim1-sgRNA ($2 \times 10^{12}$ v.g./ml) was injected into the bilateral hippocampus at a rate of 0.2 μl/min with a total volume of 1 μl according to the following coordinates: 2.1 mm anterior, ±1.8 mm lateral and 1.8 mm ventral. An empty vector AAV was used as the negative control.

### 2.13. Analysis of cell viability

HT22 cell viability was determined by a Cell Counting Kit-8 (CCK8) (Glpbio, Cat# GK10001, USA) at 450 nm using a microplate reader (model No. 680, BIO-RAD, USA). Cells viability was presented as values relative to the control group.

### 2.14. TUNEL staining

TUNEL staining was performed to examine apoptosis according to the manufacturer's instructions (Beyotime, Cat# P1090, China). Samples were permeabilized with 0.3 % Triton X-100 for 5 min, incubated for 20 min in the presence of protease K, and immersed in a solution of TUNEL reaction for 60 min at 37 °C in the dark. Afterwards, DAPI staining solution (Beyotime, Cat# C1006, China) was used to label the nuclei and the samples were photographed using a laser scan confocal microscope (FV1000, Olympus, Japan). The ratio of TUNEL-positive cells to DAPI-stained ones was calculated to determine the degree of apoptosis.

### 2.15. Immunofluorescence staining

Brain tissues were fixed in 4 % paraformaldehyde for 24 h at room temperature (RT) and dehydrated in phosphate-buffered saline (PBS) containing 30 % sucrose for 48 h at 4 °C and then coronally sectioned into 30 μm thick slices with a cryostat. Cells were fixed in 4 % paraformaldehyde for 30 min at RT. 30 μm-thick frozen coronal sections or cultured cells were first permeabilized in 0.3 % Triton X-100 for 20 min, incubated with 10 % goat serum for 1 h at RT. The sections or cells were then incubated at 4 °C overnight with the primary antibodies, including mouse anti-shank3 (Neuromab, Cat# 75344, 1:200), rabbit anti-STIM1 (1:100, Cell Signaling Technology, Cat# 5668), rabbit anti-NeuN (1:100, Abcam, Cat# ab177487). After rinsing three times with PBS, sections or cells were incubated with secondary antibodies for 2 h at RT in the dark. Slices were covered with a mounting medium containing DAPI to counterstain nuclei and imaged using a laser scan confocal microscope (FV1000, Olympus, Japan) with the same exposure settings for each group.

### 2.16. Measurement of ROS

The level of ROS in mice brain tissues was determined using 2′,7′-dichlorodihydrofluorescein diacetate (DCFH-DA) (Elabscience, Cat# E-BC-K138-F, China) [34]. Accumulation of DCF was measured using a fluorescence microplate reader (FLx800, BioTek, USA) at 500 nm of excitation wavelength and 525 nm of emission wavelength.

ROS level in HT22 cells (Institute of Biochemistry and Cell Biology, SIBS, CAS) was determined using a Cell Meter Fluorimetric Intracellular Total ROS Activity Assay Kit (AAT Bioquest, Cat# 22900, USA). The fluorescence was measured using a fluorescence microplate reader (FLx800, BioTek, USA) at 650 nm of excitation wavelength and 675 nm of emission wavelength. The cells were also imaged using a laser-scanning confocal microscope (FV1000, Olympus, Japan).

### 2.17. Antioxidant system analysis

Brain tissues and cells were collected and homogenized using ice-cold PBS. Supernatants were obtained for antioxidant system analysis. The levels of malondialdehyde (MDA) (Elabscience, Cat# E-BC-K027-M,

E-BC-K028-M, China), glutathione peroxidase (GSH-Px) (Elabscience, Cat# E-BC-K096-M, China), glutathione (GSH) (Elabscience, Cat# E-BC-K030-M, China), catalase (CAT) (Elabscience, Cat# E-BC-K031-M, China), and total superoxide dismutase (T-SOD) (Elabscience, Cat# E-BC-K019-M, China) were analyzed using assay kits following the manufacturer's instructions.

### 2.18. Enzyme-linked immunosorbent assay (ELISA) for inflammatory cytokines

The protein concentration was determined by BCA Protein Assay Kits (Thermo Fisher Scientific, Cat# 23227, USA). The inflammatory cytokines concentrations per mg protein including tumor necrosis factor (TNF) (Elabscience, Cat# E-EL-M3063, China), interleukin (IL)-6 (Elabscience, Cat# E-EL-M0044c, China), and IL-1β (Elabscience, Cat# E-EL-M0037c, China) were quantified using ELISA kits according to the manufacturer's instruction. Absorbance was measured at 450 nm using a microplate reader (model No. 680, BIO-RAD, USA).

### 2.19. Molecular docking analysis

To investigate the potential binding sites between Shank3 and STIM1, molecular docking analysis was performed using AutoDock 4.0 software [35]. The structure of the ANK domain (PDB number: 6KYK) of mouse Shank3 was downloaded as a PDB file from the RCSB Protein Data Bank, and the structure of the SOAR region of mouse STIM1 predicted by Alpahfold2 was downloaded as a PDB file from the UniProt. The protein-protein interaction was analyzed using UCSF Chimera software. The protonation state was performed using the Maestro Project of Schrödinger software. After docking, the top-scored combination mode was selected for the subsequent analysis.

### 2.20. Intracellular $Ca^{2+}$ measurement

Intracellular $Ca^{2+}$ was measured with Rhod-4 AM (AAT Bioquest, Cat# 21121, USA) according to the manufacturer's instructions. Cultured cells were incubated with 5 μM Rhod-4 AM for 60 min in Hanks' Buffer with 20 mM Hepes (HHBS) buffer with 0.04 % Pluronic F-127 (Beyotime, Cat# ST501-0.1g, China). Then the dye working solution was replaced with HHBS containing 1 mM probenecid to remove any excess probes. Cells were imaged using an inverted fluorescence microscope (FV1000, Olympus, Japan) by monitoring the fluorescence intensity at Ex/Em = 540/590 nm with the same exposure settings for each comparison group. To obtain a stable $Ca^{2+}$ baseline, cells were kept in $Ca^{2+}$-free Tyrode solution for 2 min. Then 5 μm thapsigargin (TG) (MedChemExpress, Cat# HY-13433, USA) was added to induce depletion of intracellular $Ca^{2+}$ store. After 5 min, $Ca^{2+}$ influx was induced by adding 1 mM Calcium chloride solution. Rhod-4 fluorescence was measured and analyzed for 10 min.

### 2.21. Co-immunoprecipitation (Co-IP)

Brain tissues or cultured cells were harvested in a lysis buffer (Beyotime, Cat# P0013, China) containing a protease and phosphatase inhibitor cocktail (Beyotime, Cat# 1045, China) at 4 °C for 4 h, and centrifuged at 4 °C (12 000 rpm) for 10 min. According to the manufacturer's instructions, Co-IP experiments were performed using the Pierce™ Crosslink Magnetic Co-IP Kit (Thermo Fisher Scientific, Cat# 26149, USA). Magnetic beads were crosslinked with non-specific rabbit (1:50, Abclonal, Cat# AC005, China) or mouse IgG (1:50, Abclonal, Cat# AC011, China), rabbit anti-Shank3 (1:50, Cell Signaling Technology, Cat# 64555, USA), mouse anti-STIM1 (1:50, Thermo Fisher Scientific, Cat# MA1-19451, USA), rabbit anti-HA (1:100, Proteintech Group, Cat# 51064-2-AP, USA). The beads were then washed three times with coupling buffer. The protein extracts mixed with the beads were incubated overnight at 4 °C. Following the magnetic isolation, the precipitates were eluted with elution buffer, neutralized with neutralization buffer, and prepared for Western blot.

### 2.22. Protein expression

PGEX-6p-1 plasmids encoding GST, GST tagged ANK domain of Shank3 (residues 148–345, UniProtKB: Q4ACU6 · SHANK3_MOUSE) and pET32a plasmid encoding $His_6$, $His_6$ tagged SOAR domain of STIM1 (residues 334–444, UniProtKB: P70302 · STIM1_MOUSE) were transformed into Escherichia coli BL21-CodonPlus. E. coli cells were induced with 0.1 mM isopropyl β-D-thiogalactopyranoside (IPTG) and cultured in Luria broth at 18 °C for 12 h until $D_{600}$ nm reached 0.4–0.6. BL21 cells were then harvested, sonicated in cold PBS, and purified with Glutathione S-transferase (GenScript, Cat# L00206, China) beads or Nickel-nitrilotriacetic acid (GenScript, Cat# L00250, China) beads according to the users' manual. Efficiency of purification was verified by SDS-PAGE, followed by Coomassie blue staining.

Mouse Shank3-ANK (148–345) and STIM1-SOAR (334–444) were cloned into the pcDNA3.1 vector. The HA-ANK protein and the HA-SOAR protein were over-expressed using HT22 cells. HA-ANK mutant was generated in the Shank3-ANK (148–345) sequence and constructed by knocking out the predicted binding sites according to the molecular docking assays.

### 2.23. GST (glutathione S-transferase) pull-down assays

For GST pull-down assays, an equal amount (0.5 mg) of purified ANK domain of Shank3-GST fusion protein and SOAR domain of STIM1- $His_6$ fusion protein were mixed and incubated on ice for 3 h. Subsequently, the mixture was loaded onto Glutathione Sepharose 4B resin columns. After being washed five times with wash buffer, the proteins were eluted with wash buffer containing 15 mM reduced glutathione. The eluates were separated using 12 % SDS-PAGE, transferred to PVDF membranes, and probed with mouse anti-His (1:5000, CUSABIO, Cat# CSB-MA000159, USA) and mouse anti-GST (1:5000, CUSABIO, Cat# CSB-MA000304, USA) antibodies. The GST tag and $His_6$ tag from Wuhan GeneCreate Biological Engineering Co., Ltd. (China) were negative controls.

### 2.24. Western blot analysis

Hippocampus tissues or cultured cells were harvested for whole-cell protein extraction using ice-cold RIPA lysis buffer (Beyotime, Cat# P0013B, China) with protease and phosphatase inhibitor cocktail added. Protein concentration was quantified using the BCA kit (Beyotime, Cat# P0012, China). Equivalent amounts of protein were loaded and separated by 10 % SDS-polyacrylamide gel and transferred onto polyvinylidene difluoride (PVDF) membranes. The membranes were blocked with 5 % non-fat milk solution in tris-buffered saline with 0.1 % Triton X-100 for 1 h and then incubated overnight at 4 °C with primary antibodies against Shank3 (1:1000, Cell Signaling Technology, Cat# 64555, USA), β-actin (1:2000, Cell Signaling Technology, Cat# 3700, USA), Bax (1:1000, Cell Signaling Technology, Cat# 41162, USA), Bcl-2 (1:1000, Cell Signaling Technology, Cat# 3498, USA), cleaved-caspase3 (1:1000, Cell Signaling Technology, Cat# 9664, USA), HA (1:5000, Proteintech Group, Cat# 51064-2-AP, USA), GFP (1:20000, Proteintech Group, Cat# 66002-1-Ig, USA), STIM1 (1:1000, Thermo Fisher Scientific, Cat# MA1-19451, USA), ubiquitin (1:1000, Proteintech Group, Cat# 10201-2-AP, USA), Nrf2 (1:1000, Cell Signaling Technology, Cat# 12721, USA), Nrf2 (phospho S40) (1:1000, Abcam, Cat# ab76026, USA), Calcineurin A (1:1000, ABclonal, Cat# A4346, China), NQO1 (1:1000, ABclonal, Cat# A19586, China), and NQO1 (1:1000, ABclonal, Cat# A19062, China). Afterwards, the membranes were washed and then incubated for 1 h at RT with HRP-linked secondary antibody goat anti-rabbit IgG (1:1000, Proteintech Group, Cat# SA00003-2, USA) or goat anti-mouse IgG (1:1000, Proteintech Group, Cat# SA00001-1, USA). Protein bands

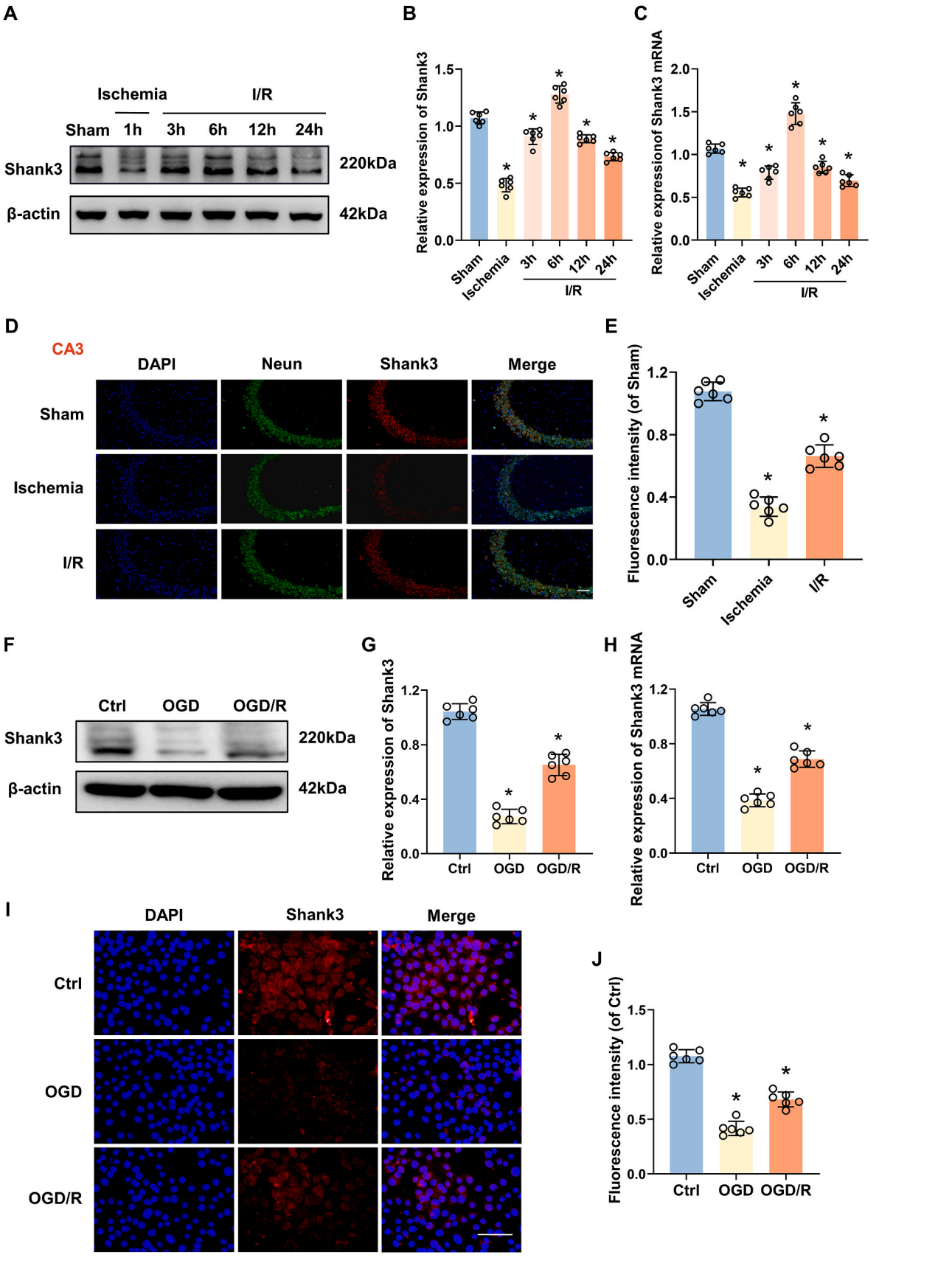


*(caption on next page)*

**Fig. 1.** The spatiotemporal expression of Shank3 in cerebral ischemia-reperfusion injury. (A) Western blot analysis of Shank3 protein levels in tissue extracts of mouse hippocampus after 60 min tMCAO followed by 3, 6, 12, and 24 h of reperfusion. (B) Quantification of Shank3 gray value relative to β-actin [n = 6, F [5,30] = 141.7, $P < 0.0001$]. (C) The qRT-PCR analysis of Shank3 mRNA levels isolated from the hippocampus after ischemia-reperfusion [n = 6, F [5,30] = 104.1, $P < 0.0001$]. (D) Representative immunofluorescence staining of Shank3 (Red) and NeuN (Green) in hippocampus regions after ischemia and reperfusion, Scale bar = 50 μm. (E) Fluorescence intensity analysis of Shank3 staining [n = 6, F [2,15] = 196.0, $P < 0.0001$]. (F) Western blot analysis of Shank3 protein levels in HT22 cells subjected to OGD for 8 h and reperfusion for 24 h. (G) Quantification of Shank3 gray value relative to β-actin [n = 6, F [2,15] = 218.9, $P < 0.0001$]. (H) The qRT-PCR analysis of Shank3 mRNA levels in HT22 cells after OGD/R [n = 6, F [2,15] = 252.3, $P < 0.0001$]. (I) Immunofluorescence staining of Shank3 (Red) and NeuN (Green) in HT22 cells after OGD and reperfusion, Scale bar = 100 μm. (J) Fluorescence intensity analysis of Shank3 staining [n = 6, F [2,15] = 159.2, $P < 0.0001$]. Statistical analysis was performed using one-way ANOVA followed by *post hoc* Tukey's test for multiple comparisons. Values are expressed as mean ± SD. *$P < 0.05$ indicated that the difference between the two groups was statistically significant.

were visualized by ChemiDoc MP Imaging System (Bio-Rad, USA). The optical density of each band was quantified using Image J software and normalized to β-actin densities for the same samples.

### 2.25. Statistical analysis

All the experiments were performed for at least three times and data were presented as mean ± SD, with N representing the number of independent biological replicate experiments. Statistical analysis was carried out with GraphPad Prism version 9.0 software. All the data passed normality and lognormality tests. Significant differences between the two groups were tested by unpaired *t*-test. Differences were assessed by one-way ANOVA across three or more groups, followed by *post hoc* Tukey's test for multiple comparisons. $P < 0.05$ was considered statically significant.

## 3. Results

### 3.1. Shank3 regulates in a time-dependent manner after ischemia/reperfusion (I/R) injury in vivo and in vitro

To mimic I/R injury after stroke *in vivo*, mice were subjected to tMCAO for 1 h, followed by reperfusion. As it has been reported that in the rodent brain, the hippocampus is fairly susceptible to I/R injuries [5], we focused on Shank3 expression in the hippocampus. Shank3 expression changed in a time-dependent manner both in protein and mRNA levels, which was consistent with prior studies [24]. Shank3 expression in the hippocampus dropped at 1 h after ischemia compared with the Sham group and began to rise at 3 h during the reperfusion, peaked at 6 h and dropped afterwards (Fig. 1A–C). Reperfusion 24 h was then chosen for further studies. The immunofluorescent staining of Shank3 in the hippocampus also indicated that Shank3 significantly downregulated in the ischemia and I/R groups compared with that in the Sham group (Fig. 1D and E). Accordingly, oxygen and glucose deprivation (OGD) in HT22 cells also contributed to a significant decrease in Shank3 expression. After reperfusion, Shank3 expression increased compared with it in the OGD group, although was lower than that in cells cultured in standard condition (Control group) (Fig. 1F–J). These data indicated that I/R results in a time-dependent fluctuation in Shank3 expression both *in vivo* and *in vitro*.

### 3.2. Neuron-specific Shank3 knockout aggravates brain injuries after I/R by promoting neuronal apoptosis

To further investigate the roles of Shank3 in I/R-induced neuronal injury, neuron-specific Shank3 knockout mice ($Shank3^{cko}$) generated using the Cre-LoxP recombination approach (Fig. 2A) were used to construct a MCAO/R model. The knockout efficiency of Shank3 in hippocampal neurons was confirmed using Western blot and immunofluorescence (Suppl Fig. 1A-D). Although $Shank3^{cko}$ mice showed partial neurological deficits (Suppl Fig. 1E-H), Sham operation had limited effects on $Shank3^{cko}$ mice in the focal score, brain infarction, and edema except for the general score (Fig. 2B–F). Compared with $Shank3^{f/f}$ mice, $Shank3^{cko}$ mice showed significantly severer neurological deficits, increased brain edema and infarct volume ratio after I/R (Fig. 2B–F). Western blot results showed that the levels of the anti-apoptotic marker, Bcl-2/Bax ratio decreased, while the apoptotic marker cleaved-caspase3 increased after I/R in the $Shank3^{cko}$ mice (Fig. 2G–I). Similarly, Shank3 deficiency increased the number of TUNEL-positive cells in the hippocampus after I/R (Fig. 2J and K). These results indicated that knockout of Shank3 in neurons aggravates brain damage after I/R and induced deterioration of neurological function by promoting neuronal apoptosis.

### 3.3. Loss of Shank3 exacerbates oxidative stress and inflammation after I/R in vivo

This study investigated the effects of Shank3 on oxidative stress and inflammation given the involvement of oxidative stress and inflammation in the induction of neuronal apoptosis after I/R. The levels of lipid peroxidation products ROS and malondialdehyde (MDA) in $Shank3^{f/f}$ mice brains significantly increased after I/R compared with that in the Sham group, which further increased due to the loss of Shank3 (Fig. 3A and B). On the other hand, the levels of antioxidants, such as GSH-Px, GSH, CAT, and SOD significantly decreased with the loss of Shank3 after I/R (Fig. 3C–F). In addition, the pro-inflammatory cytokines TNF, IL-1β, and IL-6 also increased markedly with conditional Shank3 knockout (Fig. 3G–I). Measurement of cytokine levels in the serum reveled that Shank3 knockout showed a similar variation tendency as those in the tissues (Suppl Fig. 2). Thus, the results suggested that loss of Shank3 exacerbates oxidative stress and inflammation of hippocampal neurons after I/R *in vivo*.

### 3.4. Shank3 inhibits apoptosis, ROS production and inflammation after OGD/R in vitro

To elucidate the protective effect of Shank3 against ischemic reperfusion-induced cellular injury *in vitro*, Shank3 was knocked down by shRNA and overexpressed by lentivirus in HT22 cells before OGD/R. Consistent with the results of *in vivo* experiments, the loss of Shank3 *in vitro* increased apoptotic protein cleaved-caspase3 and decreased the Bcl-2/Bax ratio and cell viability of HT22 subjected to OGD/R (Fig. 4A–C, F). The increased apoptosis after Shank3 deficiency was also observed with TUNEL staining (Fig. 4D and E). Moreover, the knockdown of Shank3 significantly increased ROS and MDA and decreased the production of antioxidants including GSH-Px, GSH, and SOD after OGD/R (Fig. 4G-L). The expression of pro-inflammatory cytokines including TNF, IL-1β, and IL-6, increased after OGD/R in HT22 cells, and further increased significantly due to the loss of Shank3 (Fig. 4M − O). These above deleterious effects of OGD/R and Shank3 knockdown could be partially reversed by Shank3 overexpression (Fig. 4A-O). Taken together, these results suggest that Shank3 exerts a protective effect on cellular injury induced by oxidative stress and inflammation after OGD/R *in vitro*.

### 3.5. Shank3 directly interacts with STIM1 in neurons

To further reveal the downstream signaling influenced by Shank3, RNA-Seq on $Shank3^{cko}$ and $Shank3^{f/f}$ mice hippocampus was performed. GO analysis of changed proteins between the two groups in molecular function showed that the genes expression related to calcium ion

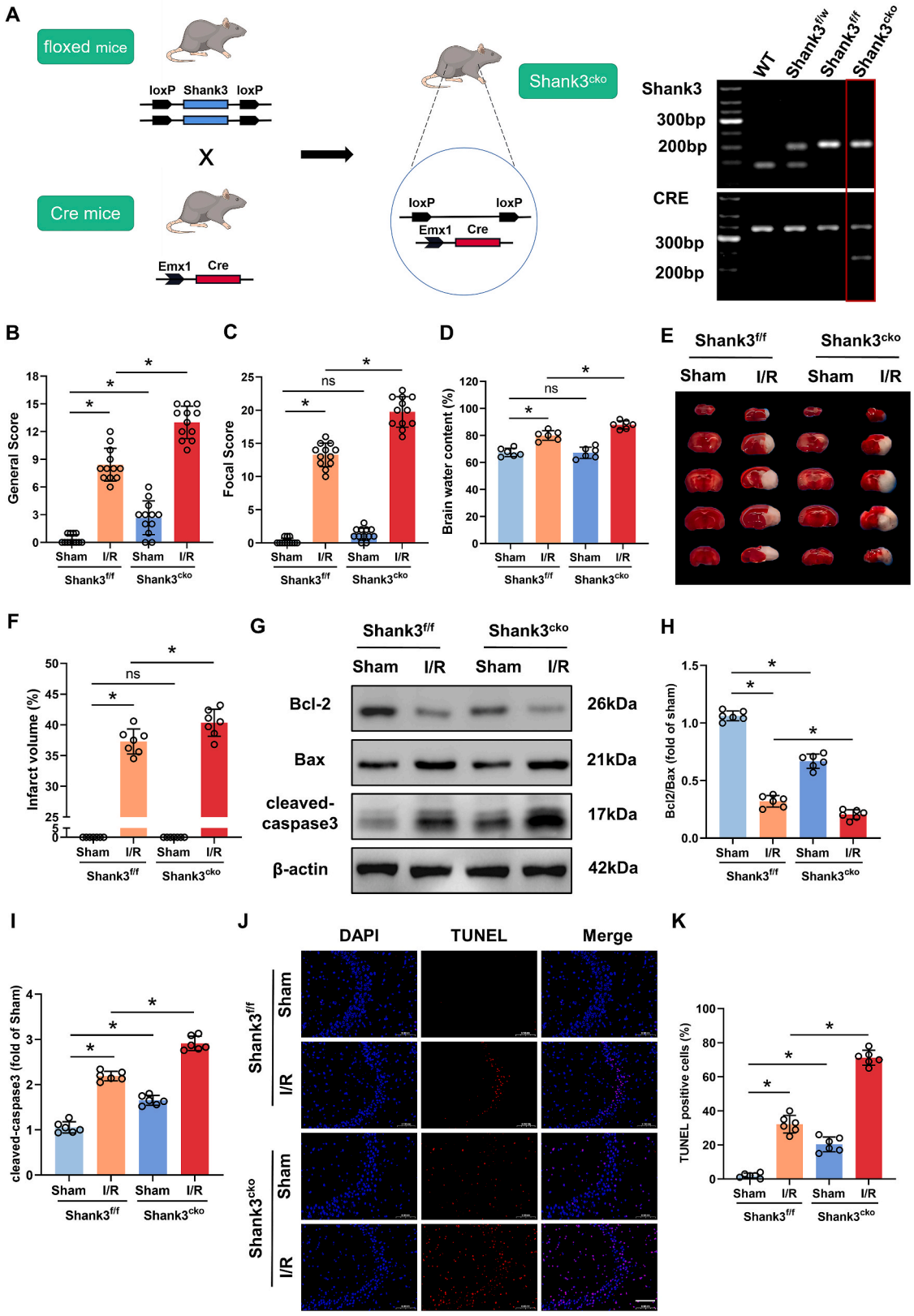


**Fig. 2.** Shank3 knockout exacerbates ischemic brain injuries. (A) Construction of conditional knockout mice of Shank3. (B, C) General [n = 12, F [3,44] = 159.4, $P < 0.0001$] and focal deficits [n = 12, F [3,44] = 456.9, $P < 0.0001$] in the Clark score after I/R. (D) Quantification of brain edema [n = 6, F [3,20] = 50.29, $P < 0.0001$]. (E, F) TTC staining indicated the infarction (white) of the brains [n = 7, F [3,24] = 1570, $P < 0.0001$]. (G–I) Western blot analysis of Bcl-2/Bax [n = 6, F [3, 20] = 359.6, $P < 0.0001$], and cleaved-caspase3 [n = 6, F [3,20] = 236.9, $P < 0.0001$] levels in tissue extracts of mouse hippocampus. (J) Representative confocal images of NeuN (Green) and TUNEL (Red) in hippocampus regions, Scale bar = 100 μm. (K) Quantitative analysis of TUNEL-positive cells [n = 6, F [3,20] = 310.4, $P < 0.0001$]. Statistical analysis was performed using one-way ANOVA followed by *post hoc* Tukey's test for multiple comparisons. Values are expressed as mean ± SD. *$P < 0.05$ indicated that the difference between the two groups was statistically significant. ns represents no statistical significance.

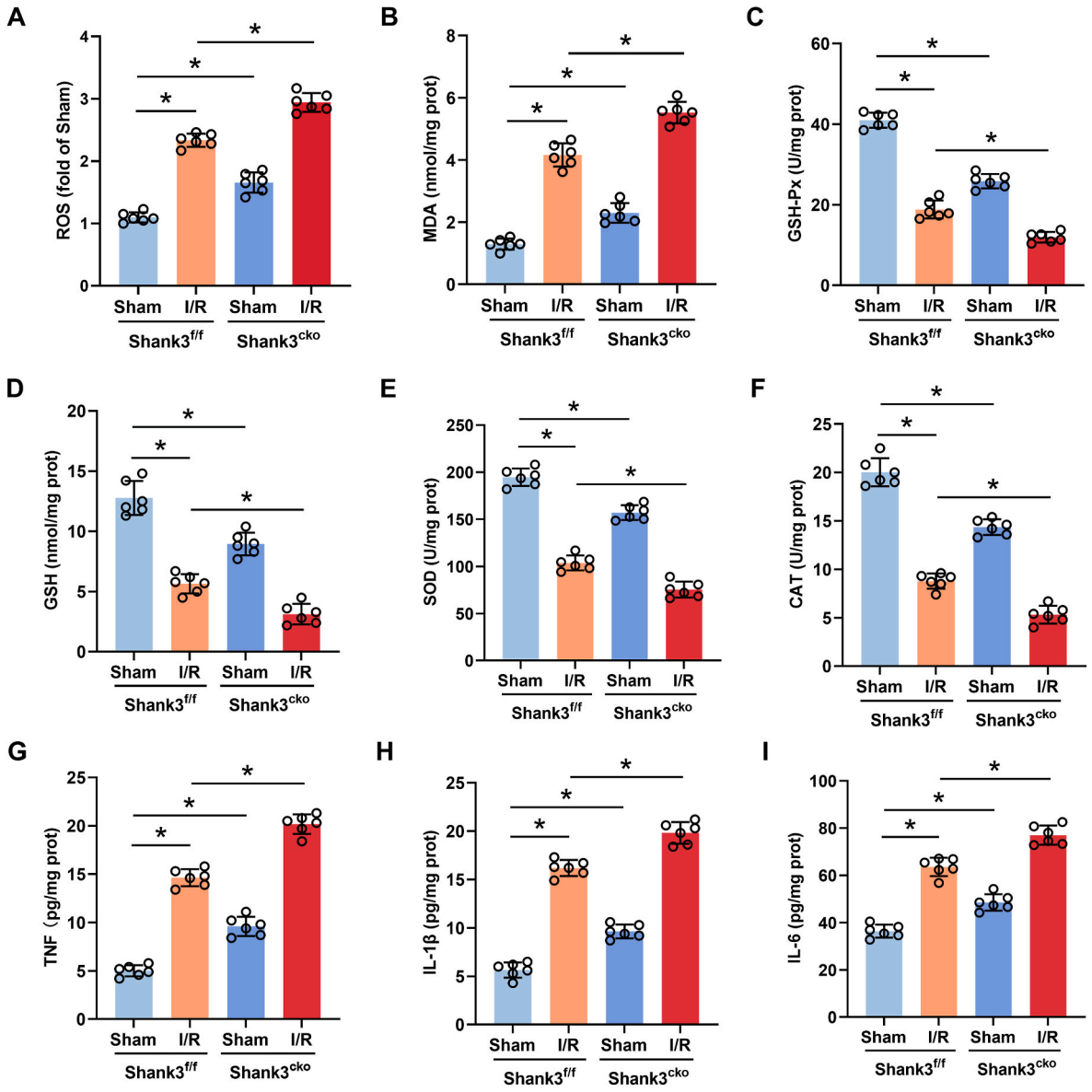


**Fig. 3.** Shank3 deficiency aggravates oxidative stress and inflammation after I/R. (A–I) The hippocampus tissues after I/R were collected and homogenized to determine the levels of ROS [n = 6, F [3,20] = 231.2, $P < 0.0001$], MDA [n = 6, F [3,20] = 218.5, $P < 0.0001$], GSH-Px [n = 6, F [3,20] = 279.6, $P < 0.0001$], GSH [n = 6, F [3,20] = 98.82, $P < 0.0001$], SOD [n = 6, F [3,20] = 240.8, $P < 0.0001$], CAT [n = 6, F [3,20] = 237.2, $P < 0.0001$], TNF [n = 6, F [3,20] = 326.6, $P < 0.0001$], IL-1β [n = 6, F [3,20] = 319.7, $P < 0.0001$], and IL-6 [n = 6, F [3,20] = 77.59, $P < 0.0001$] using assay kits. Statistical analysis was performed using one-way ANOVA followed by *post hoc* Tukey's test for multiple comparisons. Values are expressed as mean ± SD. *$P < 0.05$ indicated that the difference between the two groups was statistically significant.

binding were enriched (Suppl Fig. 3A). GSEA suggested that gene set negatively regulated cytosolic calcium ion concentration changed significantly (Suppl Fig. 3B). STIM1 is an essential $Ca^{2+}$-binding protein and intracellular $Ca^{2+}$ regulator located on endoplasmic reticulum membrane [25,36,37]. Our previous studies found that the increased expression of STIM1 was associated with neuronal oxidative injury and apoptosis [26,27], while inhibition of STIM1 alleviated calcium overload-mediated neuronal injury [28]. We thus speculate that Shank3 probably played a protective role in oxidative stress following I/R by interacting with STIM1, and in turn, reducing calcium influx. Thus, to verify whether Shank3 directly binds with STIM1 through protein-protein interactions, a molecular docking experiment was performed to detect the potential binding sites of Shank3 with STIM1 (Fig. 5A and B). The prediction results in Fig. 5C and D showed the cytoplasmic ANK domain of Shank3 directly interacted with the cytoplasmic SOAR domain of STIM1 by hydrogen bonds, salt bridges, and π-stacking. To be specific, Arg194 in the ANK domain formed salt bridges with Glu425 in the SOAR domain, while the π-stacking interaction was formed between Trp341 on SOAR and Tyr293 in the ANK domain. Moreover, the immunofluorescence test demonstrated that Shank3 and STIM1 were mainly co-localized in the cytoplasm and on the cell membrane of the hippocampal neurons (Fig. 5E). The protein-protein interaction between Shank3 and STIM1 was assessed by using co-immunoprecipitation (Co-IP) assay (Fig. 5F). Glutathione S-transferase (GST) pull-down experiments further corroborated the physical association between the ANK domain of Shank3 and the SOAR domain of STIM1 (Suppl Fig. 3C and Fig. 5G). Afterwards, the ANK domain was mutated by knocking out the binding sites predicted by molecular docking experiments. Co-IP experiments showed that the interaction between ANK-GFP and SOAR-HA was reduced significantly in the mutant cell lines (Fig. 5H and I). Lastly, the results of Western blot showed that STIM1 protein level decreased on the condition of Shank3

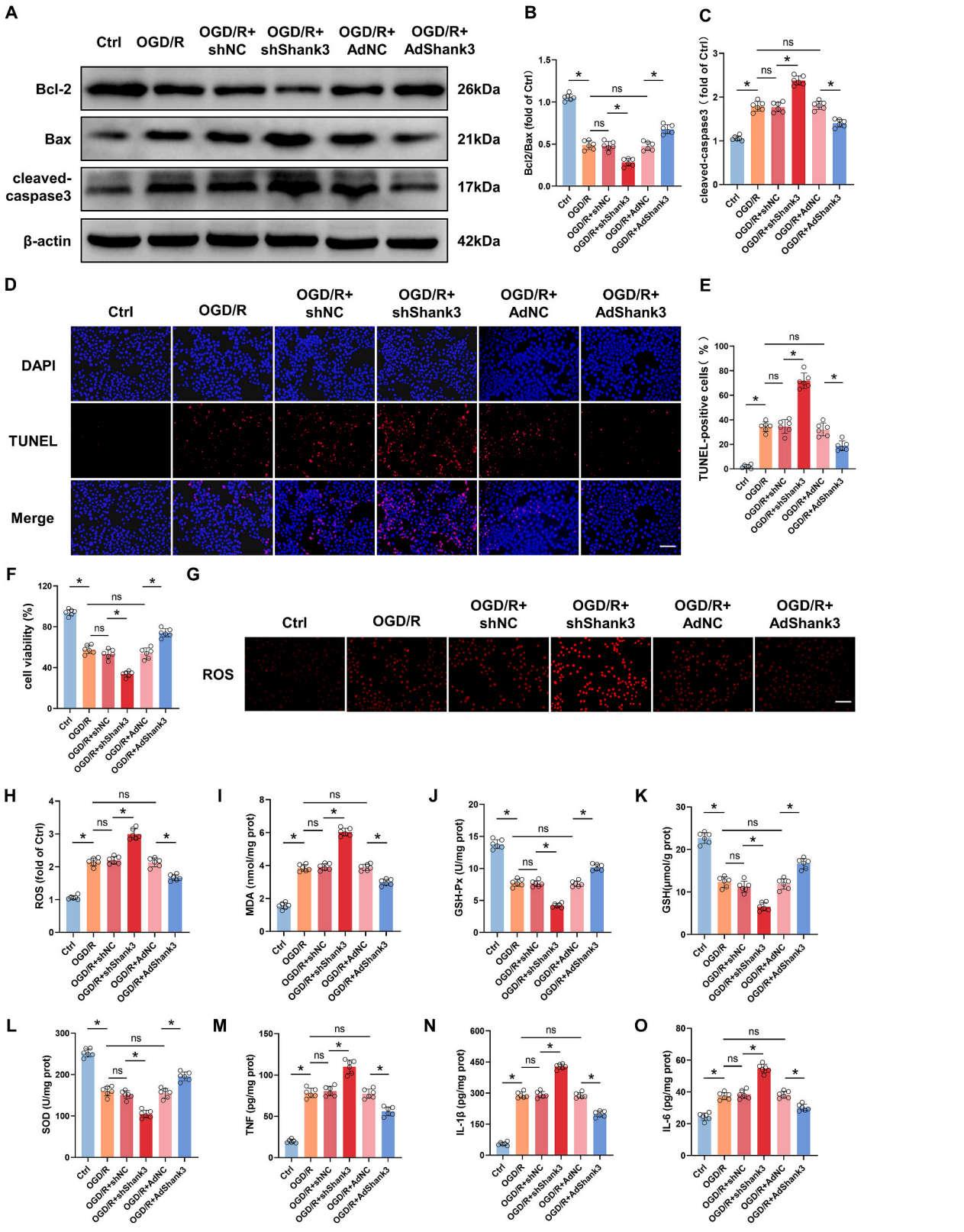


**Fig. 4.** Effects of Shank3 deficiency on the cytotoxicity and apoptosis in HT22 cells after OGD/R. (A–C) Western blot analysis of Bcl-2/Bax [n = 6, F [5,30] = 175.9, $P < 0.0001$], and cleaved-caspase3 [F [5,30] = 13.7, $P < 0.0001$] levels in HT22 cells affected by Shank3 after OGD/R. (D, E) Representative confocal images of the effect of Shank3 on TUNEL staining, Scale bar = 100 μm [n = 6, F [5,30] = 145.4, $P < 0.0001$]. (F) HT22 cells viability [n = 6, F [5,30] = 151.8, $P < 0.0001$]. (G, H) Representative Fluorescence staining images (Scale bar = 100 μm) and quantitative analysis of ROS levels [n = 6, F [5,30] = 179.6, $P < 0.0001$]. (I–O) Effects of Shank3 on MDA [n = 6, F [5,30] = 322.5, $P < 0.0001$], GSH-Px [n = 6, F [5,30] = 333.8, $P < 0.0001$], GSH [n = 6, F [5,30] = 124.5, $P < 0.0001$], SOD [n = 6, F [5, 30] = 137.5, $P < 0.0001$], TNF [n = 6, F [5,30] = 166.7, $P < 0.0001$], IL-1β [n = 6, F [5,30] = 534.9, $P < 0.0001$], and IL-6 [n = 6, F [5,30] = 109.4, $P < 0.0001$]. Statistical analysis was performed using one-way ANOVA followed by *post hoc* Tukey's test for multiple comparisons. Values are expressed as mean ± SD. *$P < 0.05$ indicated that the difference between the two groups was statistically significant. ns represents no statistical significance.

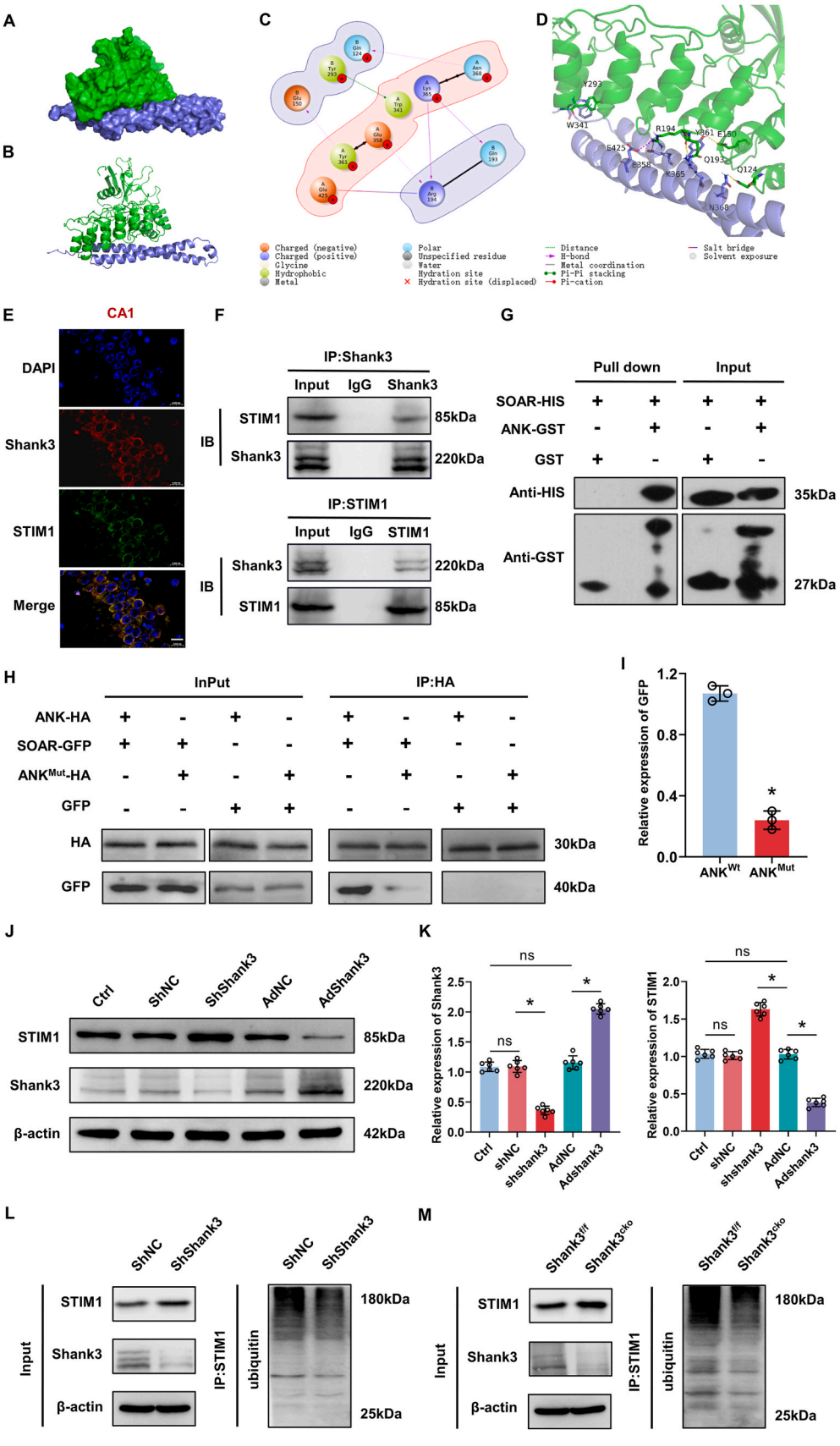


*(caption on next page)*

**Fig. 5.** Regulatory effects of Shank3 on STIM1. (A, B) Overview of Shank3 ANK domain (Green) binding to SMIT1 SOAR domain (Violet). (C, D) Predictive analysis of the binding mode of Shank3 ANK domain to SMIT1 SOAR domain in 2D and 3D. (E) Double fluorescent staining of Shank3 (Green) and STIM1 (Red) in the hippocampus, Scale bar = 100 μm. (F) Co-immunoprecipitation (Co-IP) assay suggested protein-protein interactions between Shank3 and STIM1. (G) GST pull-down assay revealed Shank3 directly bound with STIM1 (n = 3, t = 18.65, df = 4, $P < 0.0001$). (H, I) Shank3 mutant significantly reduced the protein-protein interactions between Shank3 and STIM1 [n = 3, t = 18.41, $P < 0.0001$]. (J, K) Western blot analysis of Shank3 protein levels [n = 6, F [4,25] = 259.1, $P < 0.0001$] and STIM1 protein levels [n = 6, F [4,25] = 269.9, $P < 0.0001$] in modified HT22 cells. (L, M) STIM1 ubiquitination levels in Shank3 knockdown HT22 cells and hippocampus of Shank3$^{cko}$ mice. Statistical analysis was performed using one-way ANOVA followed by *post hoc* Tukey's test for multiple comparisons and unpaired *t*-test between two groups. Values are expressed as mean ± SD.*$P < 0.05$ indicated that the difference between the two groups was statistically significant. ns represents no statistical significance.

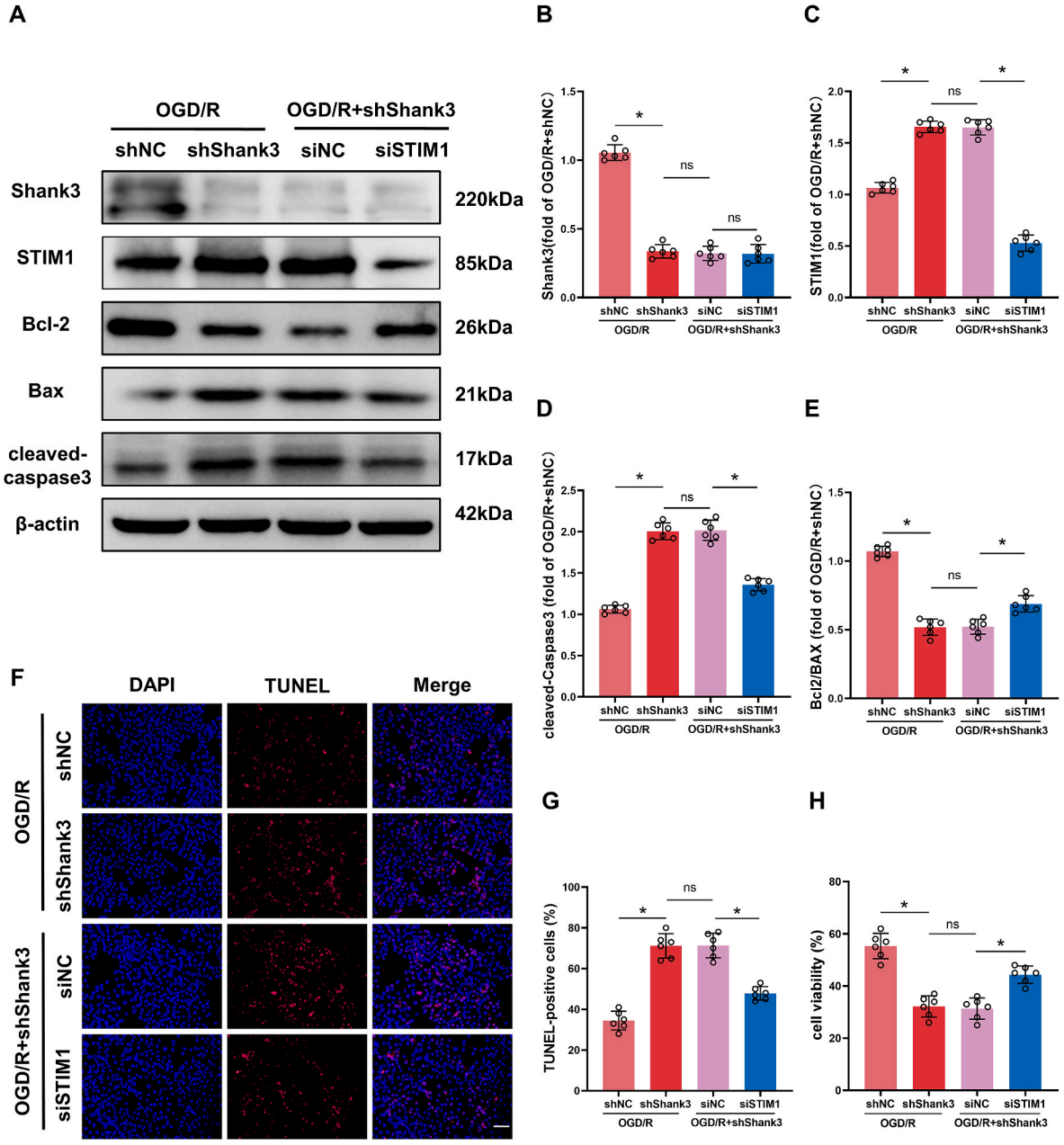


**Fig. 6.** Downregulation of STIM1 mitigates OGD/R-induced cell injury after Shank3 knockdown. (A–E) Western blot analysis of Shank3 [n = 6, F [3,20] = 248.6, $P < 0.0001$], STIM1 [n = 6, F [3,20] = 405.9, $P < 0.0001$], Bcl-2/Bax [n = 6, F [3,20] = 140.0, $P < 0.0001$], and cleaved-caspase3 [n = 6, F [3,20] = 165.5 $P < 0.0001$] levels in Shank3-knockdown cells affected by silencing STIM1 after OGD/R. (F, G) Effects of silencing STIM1 on TUNEL staining (Scale bar = 100 μm) [n = 6, F [3,20] = 76.09, $P < 0.0001$]. (H) Cells viability [n = 6, F [3,20] = 45.52, $P < 0.0001$]. Statistical analysis was performed using one-way ANOVA followed by *post hoc* Tukey's test for multiple comparisons. Values are expressed as mean ± SD. *$P < 0.05$ indicated that the difference between the two groups was statistically significant. ns represents no statistical significance.

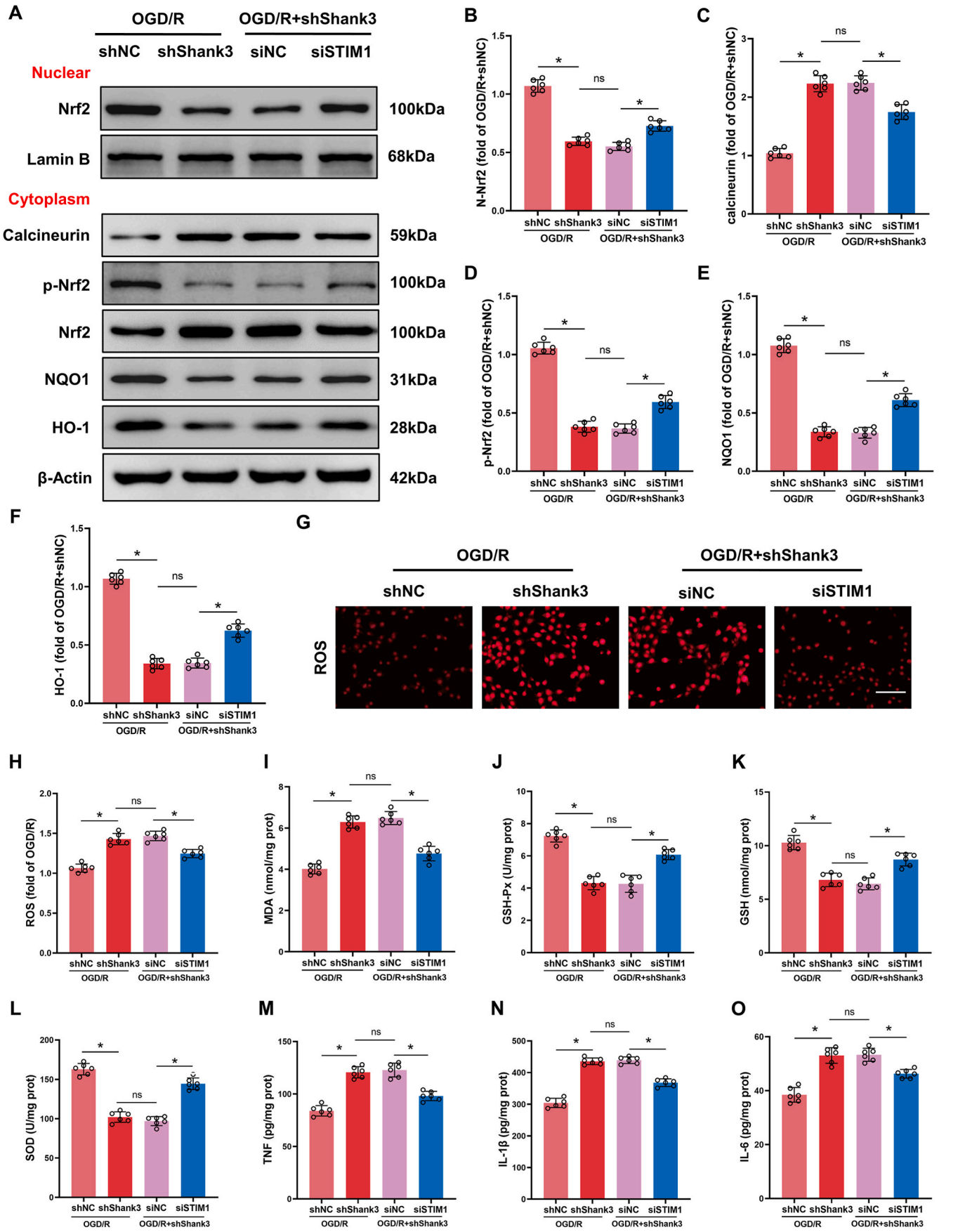


*(caption on next page)*

**Fig. 7.** The Shank3/STIM1/Nrf2 signaling pathway is involved in Nrf2 nuclear accumulation and anti-oxidative stress activity after OGD/R. (A–F) Western blot analysis of nuclear Nrf2 [n = 6, F [3,20] = 179.1, $P < 0.0001$], calcineurin [n = 6, F [3,20] = 137.5, $P < 0.0001$], p-Nrf2 [n = 6, F [3,20] = 262.6, $P < 0.0001$], NQO1 [n = 6, F [3,20] = 278.8, $P < 0.0001$] and HO-1 [n = 6, F [3,20] = 262.6, $P < 0.0001$] levels in modified cells after OGD/R. (G, H) Representative fluorescence staining images (Scale bar = 100 μm) and quantitative analysis of ROS levels [n = 6, F [3,20] = 60.28, $P < 0.0001$]. (I–L) Analysis of antioxidant system including MDA [n = 6, F [3,20] = 93.55, $P < 0.0001$], GSH-Px [n = 6, F [3,20] = 73.16, $P < 0.0001$], GSH [n = 6, F [3,20] = 51.18, $P < 0.0001$], and SOD [n = 6, F [3,20] = 134.9, $P < 0.0001$]. (M–O) Effects of knockdown STIM1 on TNF [n = 6, F [3,20] = 72.57, $P < 0.0001$], IL-1β [n = 6, F [3,20] = 170.9, $P < 0.0001$], and IL-6 [n = 6, F [3,20] = 49.04, $P < 0.0001$]. Statistical analysis was performed using one-way ANOVA followed by *post hoc* Tukey's test for multiple comparisons. Values are expressed as mean ± SD. *$P < 0.05$ indicated that the difference between the two groups was statistically significant. ns represents no statistical significance.

overexpression, while increased when Shank3 was knocked down indicating that Shank3 negatively regulated the expression of STIM1 (Fig. 5J and K).

Since it has been confirmed that Shank3 deficiency inhibited ubiquitination-dependent protein degradation [38], to further investigate whether Shank3 promotes proteasome-induced STIM1 degradation, Shank3 knockdown HT22 cells were treated with cycloheximide (CHX, protein synthesis inhibitor) and MG132 (proteasome inhibitor). This treatment revealed STIM1 protein levels decreased significantly after CHX (100 μM) treatment in the shNC group, compared with the shShank3 group (Suppl Fig. 3D and E). However, STIM1 expression did not change significantly at all the time points after the addition of MG132 (30 μM), while the expression of STIM1 in the shShank3 group remained consistently higher than that of the shNC group (Suppl Fig. 3F and G). Co-IP was then conducted to investigate the ubiquitination of STIM1. The results showed that Shank3 deficiency resulted in a decrease in the STIM1 polyubiquitination level both *in vitro* and *in vivo* (Fig. 5L and M). The results suggest that Shank3 may degrade STIM1 through the ubiquitin-proteasome pathway. The above results can validate that Shank3 directly binds with STIM1 to regulate its stability. To verify whether the loss of Shank3 can regulate STIM1-mediated $Ca^{2+}$ influx, intracellular $Ca^{2+}$ was measured with Rhod-4 AM. Confocal intracellular $Ca^{2+}$ imaging showed that STIM1-mediated $Ca^{2+}$ influx increased following OGD/R in HT22 cells, which was further enhanced by Shank3 knockdown (Suppl Fig. 3H).

### 3.6. Shank3 alleviates OGD/R-induced neuronal injury by downregulating STIM1 expression

We further explored whether the protective role of Shank3 against OGD/R-induced neuronal injury was dependent on STIM1. Downregulation of STIM1 expression (Suppl Fig. 4) partially reversed the decrease of Bcl-2/Bax ratio and upregulated cleaved-caspase3 expression induced by Shank3 knockdown after OGD/R (Fig. 6A–E). TUNEL staining and CCK-8 assay also indicate that cell apoptosis decreased, and viability increased in the STIM1 and Shank3 double knockouts group compared with that in the Shank3 knockout group (Fig. 6F–H). These results suggest that Shank3 alleviates OGD/R-induced cell injury by downregulating STIM1 *in vitro*.

### 3.7. Shank3/STIM1 interaction exerts an anti-oxidative stress role after OGD/R through Nrf2 phosphorylation and nuclear translocation

It has been accepted that the Nrf2 pathway is protective against brain injuries by inhibiting oxidative stress and inflammation [39–41]. Given this, whether the Shank3/STIM1 interaction affected oxidative stress-related downstream signaling pathways in an Nrf2-dependent manner was examined in the following study. Calcium influx was observed using confocal intracellular $Ca^{2+}$ imaging. This imaging revealed that, compared with the shNC group, Shank3 knockdown enhanced $Ca^{2+}$ influx in HT22 cells after ODG/R, which was significantly reversed by silencing STIM1 (Suppl Fig. 5A and B). Increased $Ca^{2+}$ influx induced an increase in calcineurin expression and dephosphorylation of Nrf2 (Fig. 7A–C). The decreased Nrf2 phosphorylation (p-Nrf2) inhibited Nrf2 translocating into the nuclear, and thus decreased the expression of downstream targets, such as NQO-1 and HO-1 (Fig. 7A). However, this effect was reversed by STIM1 knockdown in HT22 cells after OGD/R (Fig. 7A–F, Suppl Fig. 5C). In addition, STIM1 downregulation also reversed the effect of Shank3 deficiency on the regulation of various oxidant/antioxidant molecules, such as ROS, MDA, SOD, GSH-Px, GSH, and SOD (Fig. 7G-L), and the elevation of pro-inflammatory cytokines including TNF, IL-1β and IL-6 (Fig. 7M – O). These results suggest that the protective effect of Shank3/STIM1 interaction against OGD/R-induced oxidative stress and inflammatory activity is dependent on Nrf2 phosphorylation and nuclear translocation in neurons.

### 3.8. Knockdown of STIM1 protects Shank3$^{cko}$ mice against I/R-induced brain injuries

To further validate the effect of Shank3/STIM1 interaction *in vivo*, Shank3$^{cko}$ mice were subjected to stereotactic injection of AAV9-STIM1-sgRNA or empty vector virus into the hippocampus before tMCAO/R. Western blot confirmed the knockdown efficiency of AAV9-STIM1-sgRNA on STIM1 *in vivo* (Suppl Fig. 6). Downregulation of STIM1 significantly reduced the brain injuries as evidenced by decreased general and focal scores, infarction volume and brain edema of Shank3$^{cko}$ mice after I/R (Fig. 8A–D, Suppl Fig. 7A). In terms of cellular apoptosis, silencing of STIM1 reversed the detrimental effect of Shank3 depletion, significantly increased Bcl-2/Bax ratio, and lowered cleaved-caspase3 levels (Fig. 8E–G) and the number of TUNEL-positive cells in the mice hippocampus (Fig. 8H and I) after I/R. Additionally, levels of ROS, MDA and inflammatory cytokines declined in STIM1 deficiency mice hippocampus compared with the negative control counterparts, while the anti-oxidant enzymes GSH-Px and SOD increased (Fig. 8J-P, Suppl Fig. 7B and C). Cytokine level in the serum also suggested that silencing of STIM1 inhibited inflammatory response induced by Shank3 knockout (Suppl Fig. 8). Our findings indicate that the Shank3 interacts with STIM1 and thus protects against oxidative stress and inflammatory response after I/R.

## 4. Discussion

Ischemic stroke (IS) is the second leading cause of disability and death worldwide [42], and in China, age-standardized stroke prevalence amounted to 1115 cases per 100 000 people between 2012 and 2013, and has been increasing in the last ten years [43]. With the increasing clinical application of thrombolytic drugs and endovascular recanalization technology, the number of IS patients suffering from reperfusion-induced brain damage has significantly increased [44]. In the process secondary to the reperfusion, given the excessive oxidative stress and inflammation that can result in neuronal injuries, the underlying mechanism is yet to be elucidated. Therefore, it is essential to explore critical pathways involved in reperfusion injuries in order to develop promising therapeutic strategies for I/R.

Shank3, namely SH3 and multiple ankyrin repeat domains protein 3, is an essential neuronal post-synaptic dense (PSD) scaffold protein. It is composed of six domains: duf535, ANK, SH3, PDA, pro, and Sam [45], and plays a vital role in central nervous system diseases such as autism and Alzheimer's disease. Multiple studies have revealed that *in vivo*, Shank3 can form macromolecular complexes together with mGluRs, Homer1, NMDARs, PSD95, and CaMKII. This interaction can regulate synaptic plasticity by maintaining the balance between the levels of calcium ions and the concentration of excitatory transmitters in the

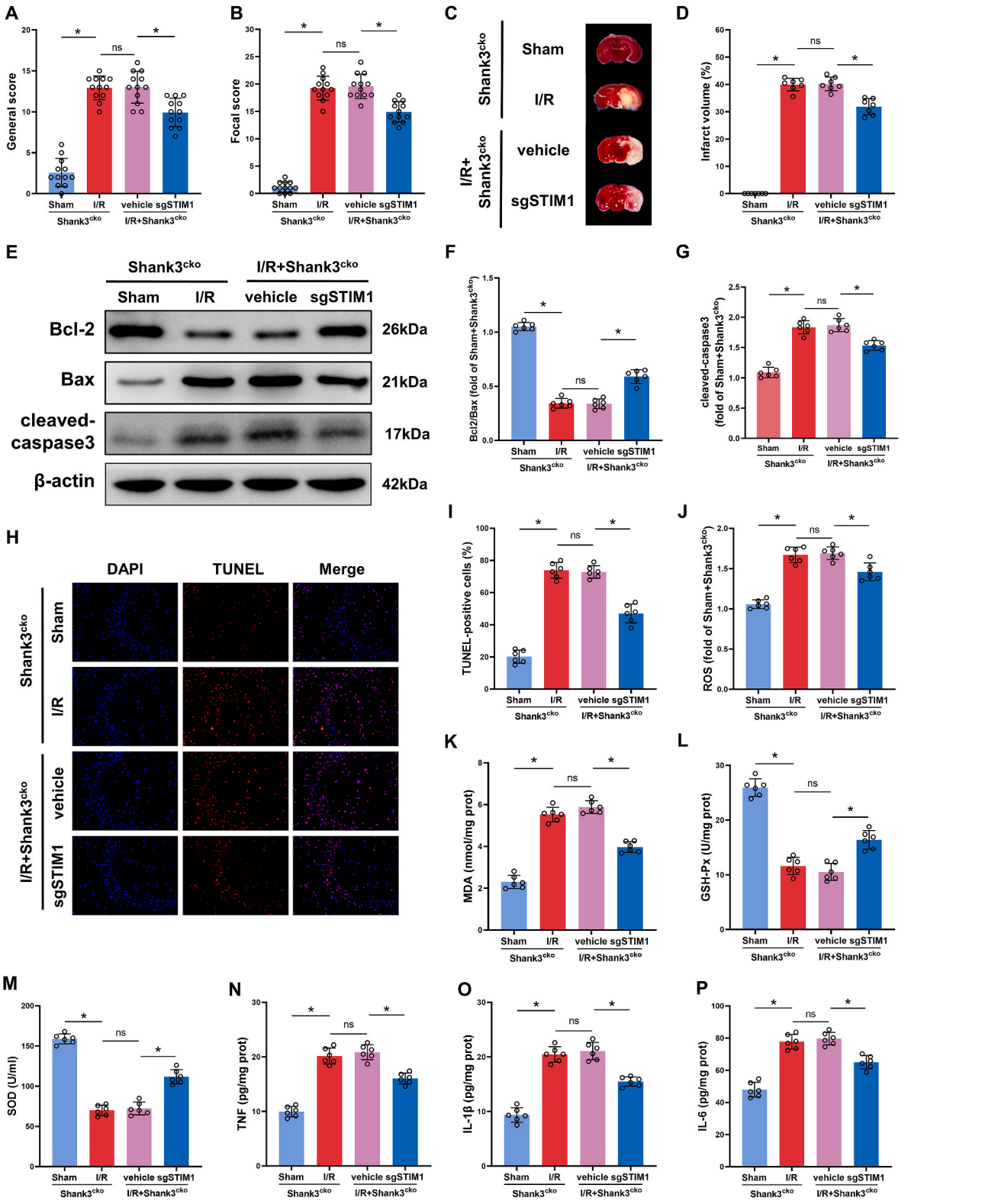


**Fig. 8.** Silencing STIM1 alleviates Shank3 deficiency-induced ischemia-reperfusion brain injuries. (A, B) General [n = 12, F [3,44] = 96.78, $P < 0.0001$] and focal [n = 12, F [3,44] = 253.1, $P < 0.0001$] deficits in the Clark score after I/R. (C, D) The infarct volume was measured with TTC staining at 24 h after tMCAO/R [n = 7, F [3,24] = 504.2, $P < 0.0001$]. (E–G) Western blot analysis of Bcl-2/Bax [n = 6, F [3,20] = 288.6, $P < 0.0001$], and cleaved-caspase3 [n = 6, F [3,20] = 84.04, $P < 0.0001$] levels. (H) Representative confocal images of NeuN (Green) and TUNEL (Red), Scale bar = 100 μm. (I) Quantitative analysis of TUNEL-positive cells [n = 6, F [3,20] = 173.1, $P < 0.0001$]. (J–P) The levels of ROS [n = 6, F [3,20] = 68.41, $P < 0.0001$], MDA [n = 6, F [3,20] = 170.0, $P < 0.0001$], GSH-Px [n = 6, F [3,20] = 114.2, $P < 0.0001$], SOD [n = 6, F [3,20] = 188.4, $P < 0.0001$], TNF [n = 6, F [3,20] = 101.2, $P < 0.0001$], IL-1β [n = 6, F [3,20] = 100.3, $P < 0.0001$], and IL-6 [n = 6, F [3,20] = 68.64, $P < 0.0001$] using assay kits. Statistical analysis was performed using one-way ANOVA followed by *post hoc* Tukey's test for multiple comparisons. Values are expressed as mean ± SD for n = 6. *$P < 0.05$ indicated that the difference between the two groups was statistically significant. ns represents no statistical significance.

brain [46–48]. Recently, Malara et al. [49–54] has found that Shank3 is involved in oligodendrocyte and astrocyte-mediated inflammatory responses and neuronal injuries in autism. Combining with our findings with that by Datta AQ that Shank3 expression decreases in rat brains after I/R [24], it is reasonable for us to speculate that Shank3 may play a protective role in I/R-induced oxidative stress and inflammation.

Multiple studies have confirmed that hippocampal neurons are highly susceptible to I/R injury [6,55–57]. Given that in the tMCAO model, the secondary cell deaths occur mainly in the hippocampus [58], in the present study, we focused on the effects of Shank3 on secondary brain injuries following oxidative stress and inflammation in the hippocampus. We discovered, for the first time, time-dependent changes in the expression of Shank3 in hippocampal neurons after I/R. Our research shows that Shank3 decreased after 1 h of ischemia, increased at least as early as 3 h after reperfusion, peaked at 6 h post-reperfusion and then decreased below the basal level. Therefore, we speculate that in the early stage after I/R, neurons may activate a self-defensive protection mechanism, upregulate the Shank3, and thus inhibit oxidative stress injury and neuroinflammation. However, as the I/R injury progresses to the later stages, the brain's self-protective ability decreases, leading to the downregulation of Shank3. We constructed a model with neuron-specific Shank3 knockout mice and based on the model, we found that Shank3 deletion aggravated the neurological deficit, brain edema and cerebral infarction volume after I/R.

The study by Xie et al. [59] showed that the polycyclic aromatic hydrocarbons phenanthrene exposure resulted in a significant decrease in Shank3 expression, a subsequent increase in ROS and a decrease in glutathione in the mouse brain. Amal et al. [60,61] also showed that in autistic mice, Shank3 mutation led to an alteration in Nitric Oxide (NO) and Protein S-nitrosylation (SNO). They speculated that the changes could affect a variety of mitochondrial proteins that regulate neuronal apoptosis and ROS metabolism, indicating that oxidative stress is involved in the pathogenesis of Shank3 mutation-induced autism spectrum disorder (ASD). In line with their findings, in the present study, we found that Shank3 deficiency aggravated oxidative stress after I/R, which was evidenced by the increased ROS content and decreased SOD and GSH-Px activity. We also found, for the first time, that Shank3 suppressed the level of pro-inflammatory cytokines such as TNF, IL-1β, and IL-6 in the neurons *in vivo* and *in vitro* after I/R.

Our RNA-Seq analysis suggests that Shank3 in hippocampal neurons can regulate calcium ion binding and cytosolic calcium ion concentration. Studies have shown that the increase in $Ca^{2+}$ concentration in the cytoplasm can induce intracellular ROS-generating enzymes to produce and generate free radicals [58,62–64], which cause oxidative stress damages, including DNA mutation, protein denaturation, and lipid peroxidation and subsequently, cell death. Casas et al. [64] found that calcium overload increased ROS levels in the brain in a NADPH Oxidases 5 (NOX5)-dependent manner after stroke. ROS can promote the production of pro-inflammatory factors through activating various signal transduction pathways such as Nuclear factor-kappa B (NF-κB) and NOD-like receptor protein 3 (NLRP3) pathway [65–68]. Intracellular calcium overload has also been demonstrated to play a vital role in mediating inflammatory responses. Yao et al. [69] identified that CaMKII-δ9/NF-κB signaling aggravated inflammation after cardiac I/R injuries. Besides, STIM1-dependent $Ca^{2+}$ entry has also been confirmed to mediate NFAT activity which was necessary for LPS-induced proinflammatory gene expression [70]. Thus, calcium overload played an essential role. in the multiple mechanisms underlying modulating oxidative stress and inflammation in post-I/R neuronal injuries.

In view of the above findings, in the present study, we focused on STIM1, a calcium ion sensor localized on the endoplasmic reticulum membrane. STIM1 interacts with the plasma membrane channel Orai1 to form the store-operated $Ca^{2+}$ entry (SOCE), which mediates calcium influx [71,72]. Our recent studies have confirmed that inhibition of SOCE can inhibit ROS accumulation and apoptosis in neuronal oxidative stress [26,27]. Additionally, our findings revealed that the expression of STIM1 was inhibited by Homer1a, which can form macromolecular complexes with Shank3. This interaction serves to attenuate glutamate-induced calcium overload [28].

In the present study, we observed that Shank3 deficiency enhanced STIM1-mediciated calcium influx under OGD/R and that downregulating STIM1 expression can reverse the Shank3-knockout-induced pro-inflammatory and pro-oxidant processes in neuronal cells after OGD/R, thus reducing ROS, MDA, TNF, IL-1β, IL-6, and increasing SOD and GSH-Px. Moreover, *in vivo* experiments showed that downregulation of STIM1 can improve the neurologic function of $Shank3^{cko}$ mice, and ameliorate the cerebral infarction and brain edema. That is to say, Shank3 can probably play a neuroprotective role after I/R by

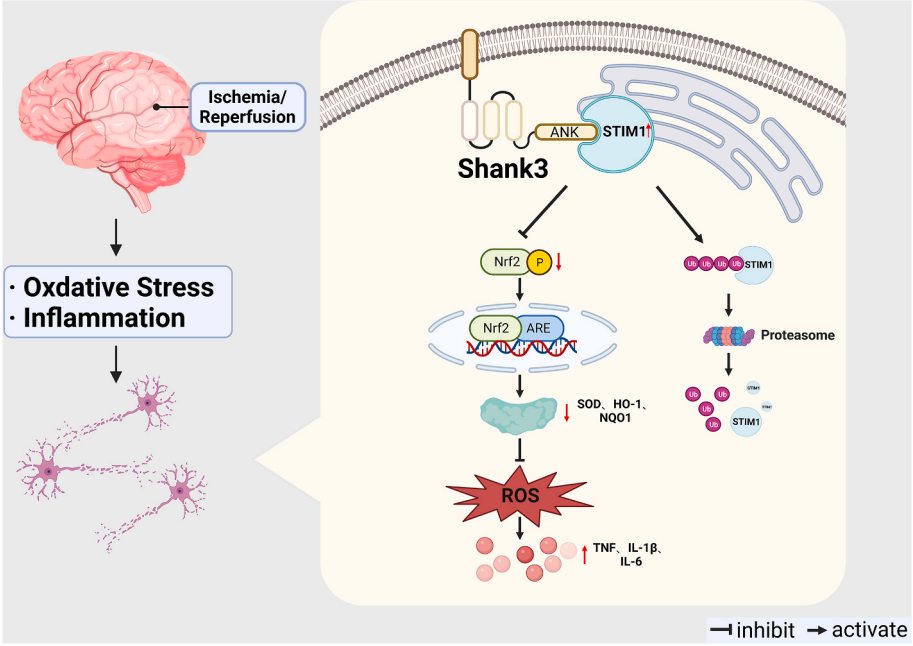


**Fig. 9.** Shank3 interacts with STIM1 and regulates post-I/R neuronal oxidative stress and inflammatory injuries through the Nrf2 pathway.

negatively regulating STIM1. We have also validated that Shank3 directly interacts with and promotes the ubiquitin-proteasome system (UPS)-mediated of STIM1 degradation, thereby alleviating neuronal oxidative injury.

The UPS-mediated degradation pathway is the main mode of protein degradation in eukaryotic cells [73]. Zhang et al. [74] were the first to report that 26S proteasome inhibitor lactacystin inhibits retinoic acid-mediated down-regulation of STIM1 protein in rat mesangial cells, and thus suggested that STIM1 can be degraded through the ubiquitin-proteasome pathway. The effect of UPS on STIM1 of HEK293 cells and primary cortical neurons was investigated, and it has been found that the proteasome inhibitor MG132 significantly increased the STIM1 level. It is widely accepted that the steady-state levels of Shank3 is related to its ubiquitination [75,76]. However, Bidinosti et al. [38] found that Shank3 can also promote ubiquitination and degradation of other proteins, such as Cdc2-like kinase 2 (CLK2). The previous research suggests that Shank3 may be involved in the regulation of STIM1 protein levels. This study shows that Shank3 knockdown reduced the degradation of STIM1, while MG132 significantly inhibited the degradation of STIM1. What's more, the polyubiquitination of STIM1 also reduced in Shank3 knockdown HT22 cells. For the first time, we uncovered that Shank3 may facilitate the degradation of STIM1 through the ubiquitin-proteasome pathway in neurons after I/R. However, further studies are warranted on how Shank3 mediates the ubiquitination of STIM1.

Nrf2 is a well-known transcriptional factor consisting of seven domains, namely Neh1-7 and regulating downstream antioxidant response element (ARE) expression. Normally, Nrf2 exists in the cytoplasm and interacts with the cysteine-rich protein Keap1 through the Neh2 domain. Phosphorylation of Neh2 domain can mediate Nrf2 nuclear translocation by affecting the dissociation of Nrf2 from Keap1 [77]. Some studies have confirmed that protein kinase (PKC) directly phosphorylates $Ser^{40}$ within the Neh2 domain, enhances Nrf2 nuclear translocation, and promotes ARE expression including SOD, heme oxygenase-1 (HO-1), and NQO1 [78–81]. Fão L et al. found that exposure of HT22 cells to $H_2O_2$ increased phosphorylation of Nrf2 $Ser^{40}$ and promoted its nuclear translocation [82]. The results of a recent research have indicated Nrf2 and STIM1 jointly regulate mitochondrial function under inflammatory condition in cardiac cells [83]. However, there is a scant amount of studies on the relationship between STIM1 and Nrf2. STIM1-induced $Ca^{2+}$ influx regulates many $Ca^{2+}$-dependent signaling molecules, including calcineurin [84,85], which dephosphorylate many downstream targets, such as Bcl-xL/Bcl-2-associated death promoter (BAD) [86,87] and nuclear factor of activated T-cells (NFA) [88,89]. Meanwhile, calcineurin can regulate cytokines production by activating downstream nuclear factor of activated T cells (NFAT), nuclear factor-kappa B (NF-κB) pathway, and so on [90,91]. For the first time, we revealed that calcineurin can dephosphorylate Nrf2, thereby reducing its antioxidant capacity. Our study discovered that in Shank3 knockdown cells after OGD/R, downregulation of STIM1 decreased the expression of calcineurin and then increased the phosphorylation of Nrf2, thereby increasing nuclear translocation of Nrf2, and the expression of antioxidant enzymes NQO 1 and HO-1. These results confirmed that Shank3 interacts with STIM1 and this interaction plays an antioxidant role by promoting Nrf2 phosphorylation.

In conclusion, the present study identified the role of Shank3 in I/R-induced neuronal oxidative stress and inflammation, and revealed the mechanism of the Shank3/STIM1/Nrf2 pathway therein (Fig. 9, created with biorender.com), thereby providing a promising therapeutic strategy for I/R.

## Funding

National Natural Science Foundation of China (No.81974188, No. 82371377), Shaanxi Creative Talents Promotion Plan-Technological Innovation Team (No. 2022TD-42), Research Fund for Young Star of Science and Technology in Shaanxi Province (No. 2023KJXX-025)

## Data and materials availability

All data were available within the manuscript and supplementary materials, or available from the corresponding author upon reasonable request.

## Author contributions

LX, ZHC, ZL and DSH worked on the experimental design. ZHC, FY, SYF and LCH conducted the experiments. WJ, WSQ, LL, XWY, YZM and YJ analyzed the data. ZHC drafted the manuscript with assistance from LX, ZL and DSH. LX, ZHC, ZL and DSH worked on the manuscript revision and data review. All the authors read and approved the final manuscript.

## Declaration of competing interest

The authors have declared that no competing interests exist.

## Data availability

Data will be made available on request.

## Acknowledgments

The authors are grateful to Dr. Qichao Huang for providing instructive advices for protein interaction, to Prof. Yue Jiang for helping to refine and polish the manuscript, to Shiyanjia Lab (www.Shiyanjia.com) for the molecular docking analysis. Thanks for the financial support from the National Natural Science Foundation of China (No. 81974188, No. 82371377), Shaanxi Creative Talents Promotion Plan-Technological Innovation Team (No. 2022TD-42), Research Fund for Young Star of Science and Technology in Shaanxi Province (No. 2023KJXX-025).

## Appendix A. Supplementary data

Supplementary data to this article can be found online at https://doi.org/10.1016/j.redox.2023.102983.

## References

[1] B.C.V. Campbell, D.A. De Silva, M.R. Macleod, S.B. Coutts, L.H. Schwamm, S. M. Davis, et al., Ischaemic stroke, Nat. Rev. Dis. Prim. 5 (1) (2019) 70.
[2] V. Saini, L. Guada, D.R. Yavagal, Global epidemiology of stroke and access to acute ischemic stroke interventions, Neurology 97 (20 Suppl 2) (2021) S6–s16.
[3] M.S. Phipps, C.A. Cronin, Management of acute ischemic stroke, BMJ (Clinical research ed) 368 (2020) l6983.
[4] E. Werden, T. Cumming, Q. Li, L. Bird, M. Veldsman, H.R. Pardoe, et al., Structural MRI markers of brain aging early after ischemic stroke, Neurology 89 (2) (2017) 116–124.
[5] Y. Maeda, M. Matsumoto, O. Hori, K. Kuwabara, S. Ogawa, S.D. Yan, et al., Hypoxia/reoxygenation-mediated induction of astrocyte interleukin 6: a paracrine mechanism potentially enhancing neuron survival, J. Exp. Med. 180 (6) (1994) 2297–2308.
[6] M.L. Smith, R.N. Auer, B.K. Siesjö, The density and distribution of ischemic brain injury in the rat following 2-10 min of forebrain ischemia, Acta Neuropathol. 64 (4) (1984) 319–332.
[7] M. Lalkovičová, V. Danielisová, Neuroprotection and antioxidants, Neural Regen Res. 11 (6) (2016) 865–874.
[8] H. Chen, Y. He, S. Chen, S. Qi, J. Shen, Therapeutic targets of oxidative/nitrosative stress and neuroinflammation in ischemic stroke: applications for natural product efficacy with omics and systemic biology, Pharmacol. Res. 158 (2020), 104877.
[9] S. Giordano, V. Darley-Usmar, J. Zhang, Autophagy as an essential cellular antioxidant pathway in neurodegenerative disease, Redox Biol. 2 (2014) 82–90.
[10] S.J. Forrester, D.S. Kikuchi, M.S. Hernandes, Q. Xu, K.K. Griendling, Reactive oxygen species in metabolic and inflammatory signaling, Circ. Res. 122 (6) (2018) 877–902.

[11] T. Chen, S.H. Dai, X. Li, P. Luo, J. Zhu, Y.H. Wang, et al., Sirt1-Sirt3 axis regulates human blood-brain barrier permeability in response to ischemia, Redox Biol. 14 (2018) 229–236.
[12] Y. Lai, P. Lin, M. Chen, Y. Zhang, J. Chen, M. Zheng, et al., Restoration of L-OPA1 alleviates acute ischemic stroke injury in rats via inhibiting neuronal apoptosis and preserving mitochondrial function, Redox Biol. 34 (2020), 101503.
[13] J. Yuan, L. Li, Q. Yang, H. Ran, J. Wang, K. Hu, et al., Targeted treatment of ischemic stroke by bioactive nanoparticle-derived reactive oxygen species responsive and inflammation-resolving nanotherapies, ACS Nano 15 (10) (2021) 16076–16094.
[14] A.M. Grabrucker, M.J. Schmeisser, M. Schoen, T.M. Boeckers, Postsynaptic ProSAP/Shank scaffolds in the cross-hair of synaptopathies, Trends Cell Biol. 21 (10) (2011) 594–603.
[15] A.M. Grabrucker, M.J. Schmeisser, P.T. Udvardi, M. Arons, M. Schoen, N. S. Woodling, et al., Amyloid beta protein-induced zinc sequestration leads to synaptic loss via dysregulation of the ProSAP2/Shank3 scaffold, Mol. Neurodegener. 6 (2011) 65.
[16] J. Peça, C. Feliciano, J.T. Ting, W. Wang, M.F. Wells, T.N. Venkatraman, et al., Shank3 mutant mice display autistic-like behaviours and striatal dysfunction, Nature 472 (7344) (2011) 437–442.
[17] R. Ortiz, M.J. Niciu, N. Lukkahati, L.N. Saligan, A.C. Nugent, D.A. Luckenbaugh, et al., Shank3 as a potential biomarker of antidepressant response to ketamine and its neural correlates in bipolar depression, J. Affect. Disord. 172 (2015) 307–311.
[18] B. Guo, J. Chen, Q. Chen, K. Ren, D. Feng, H. Mao, et al., Anterior cingulate cortex dysfunction underlies social deficits in Shank3 mutant mice, Nat. Neurosci. 22 (8) (2019) 1223–1234.
[19] J.C. Tu, B. Xiao, S. Naisbitt, J.P. Yuan, R.S. Petralia, P. Brakeman, et al., Coupling of mGluR/Homer and PSD-95 complexes by the Shank family of postsynaptic density proteins, Neuron 23 (3) (1999) 583–592.
[20] X. Wang, A.L. Bey, B.M. Katz, A. Badea, N. Kim, L.K. David, et al., Altered mGluR5-Homer scaffolds and corticostriatal connectivity in a Shank3 complete knockout model of autism, Nat. Commun. 7 (2016), 11459.
[21] C. Vicidomini, L. Ponzoni, D. Lim, M.J. Schmeisser, D. Reim, N. Morello, et al., Pharmacological enhancement of mGlu5 receptors rescues behavioral deficits in SHANK3 knock-out mice, Mol. Psychiatr. 22 (5) (2017) 689–702.
[22] T.L. Perfitt, P.E. Stauffer, K.L. Spiess, R.J. Colbran, CaMKIIα phosphorylation of Shank3 modulates ABI1-Shank3 interaction, Biochem. Biophys. Res. Commun. 524 (1) (2020) 262–267.
[23] Q. Cai, M. Zeng, X. Wu, H. Wu, Y. Zhan, R. Tian, et al., CaMKIIα-driven, phosphatase-checked postsynaptic plasticity via phase separation, Cell Res. 31 (1) (2021) 37–51.
[24] A. Datta, Q. Jingru, T.H. Khor, M.T. Teo, K. Heese, S.K. Sze, Quantitative neuroproteomics of an in vivo rodent model of focal cerebral ischemia/reperfusion injury reveals a temporal regulation of novel pathophysiological molecular markers, J. Proteome Res. 10 (11) (2011) 5199–5213.
[25] S.L. Zhang, Y. Yu, J. Roos, J.A. Kozak, T.J. Deerinck, M.H. Ellisman, et al., STIM1 is a Ca2+ sensor that activates CRAC channels and migrates from the Ca2+ store to the plasma membrane, Nature 437 (7060) (2005) 902–905.
[26] X. Li, W. Chen, L. Zhang, W.B. Liu, Z. Fei, Inhibition of store-operated calcium entry attenuates MPP(+)-induced oxidative stress via preservation of mitochondrial function in PC12 cells: involvement of Homer1a, PLoS One 8 (12) (2013), e83638.
[27] W. Rao, L. Zhang, N. Su, K. Wang, H. Hui, L. Wang, et al., Blockade of SOCE protects HT22 cells from hydrogen peroxide-induced apoptosis, Biochem. Biophys. Res. Commun. 441 (2) (2013) 351–356.
[28] W. Rao, C. Peng, L. Zhang, N. Su, K. Wang, H. Hui, et al., Homer1a attenuates glutamate-induced oxidative injury in HT-22 cells through regulation of store-operated calcium entry, Sci. Rep. 6 (2016), 33975.
[29] A.T. Dinkova-Kostova, A.Y. Abramov, The emerging role of Nrf2 in mitochondrial function, Free Radic. Biol. Med. 88 (Pt B) (2015) 179–188.
[30] J. Wang, W. Zhang, C. Lv, Y. Wang, B. Ma, H. Zhang, et al., A novel biscoumarin compound ameliorates cerebral ischemia reperfusion-induced mitochondrial oxidative injury via Nrf2/Keap1/ARE signaling, Neuropharmacology 167 (2020), 107918.
[31] M. Liu, H. Li, L. Zhang, Z. Xu, Y. Song, X. Wang, et al., Cottonseed oil alleviates ischemic stroke-induced oxidative stress injury via activating the Nrf2 signaling pathway, Mol. Neurobiol. 58 (6) (2021) 2494–2507.
[32] H.M. Shan, M. Zang, Q. Zhang, R.B. Shi, X.J. Shi, M. Mamtilahun, et al., Farnesoid X receptor knockout protects brain against ischemic injury through reducing neuronal apoptosis in mice, J. Neuroinflammation 17 (1) (2020) 164.
[33] M. Sardari, J. Skuljec, D. Yin, K. Zec, T.S. de Carvalho, D. Albers, et al., Lipopolysaccharide-induced sepsis-like state compromises post-ischemic neurological recovery, brain tissue survival and remodeling via mechanisms involving microvascular thrombosis and brain T cell infiltration, Brain Behav. Immun. 91 (2021) 627–638.
[34] S. Liao, J. Wu, R. Liu, S. Wang, J. Luo, Y. Yang, et al., A novel compound DBZ ameliorates neuroinflammation in LPS-stimulated microglia and ischemic stroke rats: role of Akt(Ser473)/GSK3β(Ser9)-mediated Nrf2 activation, Redox Biol. 36 (2020), 101644.
[35] Q. Liu, Y. Hu, Y. Cao, G. Song, Z. Liu, X. Liu, Chicoric acid ameliorates lipopolysaccharide-induced oxidative stress via promoting the keap1/nrf2 transcriptional signaling pathway in BV-2 microglial cells and mouse brain, J. Agric. Food Chem. 65 (2) (2017) 338–347.
[36] Y. Baba, K. Nishida, Y. Fujii, T. Hirano, M. Hikida, T. Kurosaki, Essential function for the calcium sensor STIM1 in mast cell activation and anaphylactic responses, Nat. Immunol. 9 (1) (2008) 81–88.
[37] W. Zhang, Y. Sun, Y. Yang, Y. Chen, Impaired intracellular calcium homeostasis enhances protein O-GlcNAcylation and promotes vascular calcification and stiffness in diabetes, Redox Biol. 63 (2023), 102720.
[38] M. Bidinosti, P. Botta, S. Krüttner, C.C. Proenca, N. Stoehr, M. Bernhard, et al., CLK2 inhibition ameliorates autistic features associated with SHANK3 deficiency, Science 351 (6278) (2016) 1199–1203.
[39] S. Dai, J. Wei, H. Zhang, P. Luo, Y. Yang, X. Jiang, et al., Intermittent fasting reduces neuroinflammation in intracerebral hemorrhage through the Sirt3/Nrf2/HO-1 pathway, J. Neuroinflammation 19 (1) (2022) 122.
[40] K. Shen, Y. Jia, X. Wang, J. Zhang, K. Liu, J. Wang, et al., Exosomes from adipose-derived stem cells alleviate the inflammation and oxidative stress via regulating Nrf2/HO-1 axis in macrophages, Free Radic. Biol. Med. 165 (2021) 54–66.
[41] A. Cuadrado, A.I. Rojo, G. Wells, J.D. Hayes, S.P. Cousin, W.L. Rumsey, et al., Therapeutic targeting of the NRF2 and KEAP1 partnership in chronic diseases, Nat. Rev. Drug Discov. 18 (4) (2019) 295–317.
[42] A. Ajoolabady, S. Wang, G. Kroemer, J.M. Penninger, V.N. Uversky, D. Pratico, et al., Targeting autophagy in ischemic stroke: from molecular mechanisms to clinical therapeutics, Pharmacol. Ther. 225 (2021), 107848.
[43] S. Wu, B. Wu, M. Liu, Z. Chen, W. Wang, C.S. Anderson, et al., Stroke in China: advances and challenges in epidemiology, prevention, and management, Lancet Neurol. 18 (4) (2019) 394–405.
[44] M. Smith, U. Reddy, C. Robba, D. Sharma, G. Citerio, Acute ischaemic stroke: challenges for the intensivist, Intensive Care Med. 45 (9) (2019) 1177–1189.
[45] P. Monteiro, G. Feng, SHANK proteins: roles at the synapse and in autism spectrum disorder, Nat. Rev. Neurosci. 18 (3) (2017) 147–157.
[46] S. Okabe, Molecular anatomy of the postsynaptic density, Mol. cellular neurosci. 34 (4) (2007) 503–518.
[47] R.D. Emes, S.G. Grant, Evolution of synapse complexity and diversity, Annu. Rev. Neurosci. 35 (2012) 111–131.
[48] R. Lin, L.N. Learman, M.A. Bangash, T. Melnikova, E. Leyder, S.C. Reddy, et al., Homer1a regulates Shank3 expression and underlies behavioral vulnerability to stress in a model of Phelan-McDermid syndrome, Cell Rep. 37 (7) (2021), 110014.
[49] M. Malara, A.K. Lutz, B. Incearap, H.F. Bauer, S. Cursano, K. Volbracht, et al., SHANK3 deficiency leads to myelin defects in the central and peripheral nervous system, Cell. Mol. Life Sci. : CMLS 79 (7) (2022) 371.
[50] G. Chana, L. Laskaris, C. Pantelis, P. Gillett, R. Testa, D. Zantomio, et al., Decreased expression of mGluR5 within the dorsolateral prefrontal cortex in autism and increased microglial number in mGluR5 knockout mice: pathophysiological and neurobehavioral implications, Brain Behav. Immun. 49 (2015) 197–205.
[51] P.N. Alexandrov, Y. Zhao, V. Jaber, L. Cong, W.J. Lukiw, Deficits in the proline-rich synapse-associated Shank3 protein in multiple neuropsychiatric disorders, Front. Neurol. 8 (2017) 670.
[52] Y. Zhao, N.M. Sharfman, V.R. Jaber, W.J. Lukiw, Down-regulation of essential synaptic components by GI-tract microbiome-derived lipopolysaccharide (LPS) in LPS-treated human neuronal-glial (HNG) cells in primary culture: relevance to Alzheimer's disease (AD), Front. Cell. Neurosci. 13 (2019) 314.
[53] K. Li, L. Li, B. Cui, Z. Gai, Q. Li, S. Wang, et al., Early postnatal exposure to airborne fine particulate matter induces autism-like phenotypes in male rats, Toxicol. Sci. : Official J. Soc. Toxicol. 162 (1) (2018) 189–199.
[54] C. Grasselli, A. Carbone, P. Panelli, V. Giambra, M. Bossi, G. Mazzoccoli, et al., Neural stem cells from shank3-ko mouse model autism spectrum disorders, Mol. Neurobiol. 57 (3) (2020) 1502–1515.
[55] D.M. Geddes, M.C. LaPlaca, R.S. Cargill 2nd, Susceptibility of hippocampal neurons to mechanically induced injury, Exp. Neurol. 184 (1) (2003) 420–427.
[56] T.H. Sanderson, J.M. Wider, 2-vessel occlusion/hypotension: a rat model of global brain ischemia, J. Vis. Exp. (76) (2013).
[57] E. Blanco-Suárez, M. Fiuza, X. Liu, E. Chakkarapani, J.G. Hanley, Differential Tiam1/Rac1 activation in hippocampal and cortical neurons mediates differential spine shrinkage in response to oxygen/glucose deprivation, J. Cerebr. Blood Flow Metabol. 34 (12) (2014) 1898–1906.
[58] M.J. Pérez-Álvarez, C. Maza Mdel, M. Anton, L. Ordoñez, F. Wandosell, Post-ischemic estradiol treatment reduced glial response and triggers distinct cortical and hippocampal signaling in a rat model of cerebral ischemia, J. Neuroinflammation 9 (2012) 157.
[59] J. Xie, Q. Han, Z. Wei, Y. Wang, S. Wang, M. Chen, Phenanthrene induces autism-like behavior by promoting oxidative stress and mTOR pathway activation, Toxicology 461 (2021), 152910.
[60] H. Amal, B. Barak, V. Bhat, G. Gong, B.A. Joughin, X. Wang, et al., Shank3 mutation in a mouse model of autism leads to changes in the S-nitroso-proteome and affects key proteins involved in vesicle release and synaptic function, Mol. Psychiatr. 25 (8) (2020) 1835–1848.
[61] M. Kartawy, I. Khaliulin, H. Amal, Systems biology reveals S-Nitrosylation-Dependent regulation of mitochondrial functions in mice with Shank3 mutation associated with autism spectrum disorder, Brain Sci. 11 (6) (2021).
[62] A. Görlach, K. Bertram, S. Hudecova, O. Krizanova, Calcium and ROS: a mutual interplay, Redox Biol. 6 (2015) 260–271.
[63] M. Fan, J. Zhang, C.W. Tsai, B.J. Orlando, M. Rodriguez, Y. Xu, et al., Structure and mechanism of the mitochondrial Ca(2+) uniporter holocomplex, Nature 582 (7810) (2020) 129–133.
[64] A.I. Casas, P.W. Kleikers, E. Geuss, F. Langhauser, T. Adler, D.H. Busch, et al., Calcium-dependent blood-brain barrier breakdown by NOX5 limits postreperfusion benefit in stroke, J. Clin. Invest. 129 (4) (2019) 1772–1778.
[65] R. Wang, Y. Zhu, X. Lin, C. Ren, J. Zhao, F. Wang, et al., Influenza M2 protein regulates MAVS-mediated signaling pathway through interacting with MAVS and increasing ROS production, Autophagy 15 (7) (2019) 1163–1181.

[66] E. Bang, D.H. Kim, H.Y. Chung, Protease-activated receptor 2 induces ROS-mediated inflammation through Akt-mediated NF-κB and FoxO6 modulation during skin photoaging, Redox Biol. 44 (2021), 102022.
[67] R. Zhou, A.S. Yazdi, P. Menu, J. Tschopp, A role for mitochondria in NLRP3 inflammasome activation, Nature 469 (7329) (2011) 221–225.
[68] H. Fan, H. Tian, F. Jin, X. Zhang, S. Su, Y. Liu, et al., CypD induced ROS output promotes intracranial aneurysm formation and rupture by 8-OHdG/NLRP3/MMP9 pathway, Redox Biol. 67 (2023), 102887.
[69] Y. Yao, F. Li, M. Zhang, L. Jin, P. Xie, D. Liu, et al., Targeting CaMKII-δ9 ameliorates cardiac ischemia/reperfusion injury by inhibiting myocardial inflammation, Circ. Res. 130 (6) (2022) 887–903.
[70] R.K. Gandhirajan, S. Meng, H.C. Chandramoorthy, K. Mallilankaraman, S. Mancarella, H. Gao, et al., Blockade of NOX2 and STIM1 signaling limits lipopolysaccharide-induced vascular inflammation, J. Clin. Invest. 123 (2) (2013) 887–902.
[71] H. Zhang, W. Xie, Y. Feng, J. Wei, C. Yang, P. Luo, Y. Yang, P. Zhao, X. Jiang, W. Liang, S. Dai, X. Li, Stromal interaction molecule 1-mediated store-operated calcium entry promotes autophagy through AKT/mammalian target of rapamycin pathway in hippocampal neurons after ischemic stroke, Neuroscience 514 (2023) 67–78, https://doi.org/10.1016/j.neuroscience.2023.01.036.
[72] M. Prakriya, R.S. Lewis, Store-operated calcium channels, Physiol. Rev. 95 (4) (2015) 1383–1436.
[73] C. Meyer-Schwesinger, The ubiquitin-proteasome system in kidney physiology and disease, Nat. Rev. Nephrol. 15 (7) (2019) 393–411.
[74] W. Zhang, H. Meng, Z.H. Li, Z. Shu, X. Ma, B.X. Zhang, Regulation of STIM1, store-operated Ca2+ influx, and nitric oxide generation by retinoic acid in rat mesangial cells, Am. J. Physiol. Ren. Physiol. 292 (3) (2007) F1054–F1064.
[75] J.M. Keil, Z. Shen, S.P. Briggs, G.N. Patrick, Regulation of STIM1 and SOCE by the ubiquitin-proteasome system (UPS), PLoS One 5 (10) (2010), e13465.
[76] X.L. Kuang, Y. Liu, Y. Chang, J. Zhou, H. Zhang, Y. Li, et al., Inhibition of store-operated calcium entry by sub-lethal levels of proteasome inhibition is associated with STIM1/STIM2 degradation, Cell Calcium 59 (4) (2016) 172–180.
[77] T. Liu, Y.F. Lv, J.L. Zhao, Q.D. You, Z.Y. Jiang, Regulation of Nrf2 by phosphorylation: consequences for biological function and therapeutic implications, Free Radic. Biol. Med. 168 (2021) 129–141.
[78] H.C. Huang, T. Nguyen, C.B. Pickett, Phosphorylation of Nrf2 at Ser-40 by protein kinase C regulates antioxidant response element-mediated transcription, J. Biol. Chem. 277 (45) (2002) 42769–42774.
[79] X. Cheng, S. He, J. Yuan, S. Miao, H. Gao, J. Zhang, et al., Lipoxin A4 attenuates LPS-induced mouse acute lung injury via Nrf2-mediated E-cadherin expression in airway epithelial cells, Free Radic. Biol. Med. 93 (2016) 52–66.
[80] A. Gallego-Selles, M. Martin-Rincon, M. Martinez-Canton, M. Perez-Valera, S. Martín-Rodríguez, M. Gelabert-Rebato, et al., Regulation of Nrf2/Keap1 signalling in human skeletal muscle during exercise to exhaustion in normoxia, severe acute hypoxia and post-exercise ischaemia: influence of metabolite accumulation and oxygenation, Redox Biol. 36 (2020), 101627.
[81] H. Zeng, L. Wang, J. Zhang, T. Pan, Y. Yu, J. Lu, et al., Activated PKB/GSK-3β synergizes with PKC-δ signaling in attenuating myocardial ischemia/reperfusion injury via potentiation of NRF2 activity: therapeutic efficacy of dihydrotanshinone-I, Acta Pharm. Sin. B 11 (1) (2021) 71–88.
[82] L. Fão, S.I. Mota, A.C. Rego, c-Src regulates Nrf2 activity through PKCδ after oxidant stimulus, Biochim. Biophys. Acta Mol. Cell Res. 1866 (4) (2019) 686–698.
[83] Y. Li, Y.F. Feng, X.T. Liu, Y.C. Li, H.M. Zhu, M.R. Sun, et al., Songorine promotes cardiac mitochondrial biogenesis via Nrf2 induction during sepsis, Redox Biol. 38 (2021), 101771.
[84] M. Vaeth, M. Maus, S. Klein-Hessling, E. Freinkman, J. Yang, M. Eckstein, et al., Store-operated Ca(2+) entry controls clonal expansion of T cells through metabolic reprogramming, Immunity 47 (4) (2017) 664, 79.e6.
[85] Z.D. Zhu, T. Yu, H.J. Liu, J. Jin, J. He, SOCE induced calcium overload regulates autophagy in acute pancreatitis via calcineurin activation, Cell Death Dis. 9 (2) (2018) 50.
[86] H.G. Wang, N. Pathan, I.M. Ethell, S. Krajewski, Y. Yamaguchi, F. Shibasaki, et al., Ca2+-induced apoptosis through calcineurin dephosphorylation of BAD, Science 284 (5412) (1999) 339–343.
[87] G.M. Cereghetti, V. Costa, L. Scorrano, Inhibition of Drp1-dependent mitochondrial fragmentation and apoptosis by a polypeptide antagonist of calcineurin, Cell Death Differ. 17 (11) (2010) 1785–1794.
[88] F. Macian, NFAT proteins: key regulators of T-cell development and function, Nat. Rev. Immunol. 5 (6) (2005) 472–484.
[89] I.A. Graef, F. Wang, F. Charron, L. Chen, J. Neilson, M. Tessier-Lavigne, et al., Neurotrophins and netrins require calcineurin/NFAT signaling to stimulate outgrowth of embryonic axons, Cell 113 (5) (2003) 657–670.
[90] J.L. Furman, C.M. Norris, Calcineurin and glial signaling: neuroinflammation and beyond, J. Neuroinflammation 11 (2014) 158.
[91] T. Meyer, D. Shimon, S. Youssef, G. Yankovitz, A. Tessler, T. Chernobylsky, et al., NAD(+) metabolism drives astrocyte proinflammatory reprogramming in central nervous system autoimmunity, Proc. Natl. Acad. Sci. U.S.A. 119 (35) (2022), e2211310119.